Journal of Computational Physics **174,** 870–902 (2001)
doi:10.1006/jcph.2001.6942, available online at http://www.idealibrary.com on IDEAL®

Program Burn Algorithms Based on Detonation Shock Dynamics: Discrete Approximations of Detonation Flows with Discontinuous Front Models

J. B. Bdzil, D. S. Stewart,[1] and T. L. Jackson

DX-division, Los Alamos National Laboratory, Los Alamos, New Mexico 87545; and Theoretical and Applied Mechanics, University of Illinois and Center for Simulation of Advanced Rockets, University of Illinois, Urbana, Illinois
E-mail: jbb@lanl.gov; dss@uiuc.edu

Received January 5, 2001; revised September 14, 2001

In the design of explosive systems, the generic problem that one must consider is the propagation of a well-developed detonation wave sweeping through an explosive charge with a complex shape. At a given instant of time, the lead detonation shock is a surface that occupies a region of the explosive and has a dimension that is characteristic of the explosive device, typically on the scale of meters. The detonation shock is powered by a detonation reaction zone, sitting immediately behind the shock, which is on the scale of 1 mm or less. Thus, the ratio of the reaction zone thickness to the device dimension is on the order of $1/1000$ or less. This scale disparity can lead to great difficulties in computing three-dimensional detonation dynamics. An attack on the dilemma in the computation of detonation systems has led to the invention of subscale models for a propagating detonation front that we refer to herein as program burn models. The program burn model does not resolve the fine scale of the reaction zone; instead the goal is to solve for the hydrodynamics of the inert product gases on a coarse grid scale, which is insufficient to resolve the physical reaction zone. We first show that traditional program burn algorithms for detonation hydrocodes used for explosive design are inconsistent and yield incorrect shock dynamic behavior. To overcome these inconsistencies, we discuss a new class of program burn models based on detonation shock dynamic theory. This new class yields more consistent and robust algorithms that better reflect the correct shock dynamic behavior.

[1] To whom correspondence should be addressed.

0021-9991/01 $35.00

1. INTRODUCTION

In the design of explosive systems, the generic problem is the propagation of a well-developed detonation wave through an explosive charge with a complex shape. At any fixed time the lead detonation shock is a surface that has dimensions on the scale of the explosive device, typically on the scale of meters. The detonation shock is powered by a reaction zone behind the lead shock, which is on the scale of 1 mm or less. The ratio of the reaction zone thickness to the device dimension is on the order of $1/1000$ or less and this scale disparity leads to great difficulties in computing three-dimensional (3D) detonation dynamics. An excellent introduction to detonation systems and applications is described by Davis in [1], and the physics of detonation phenomena is expertly described in the classic text by Fickett and Davis [2].

Assume (as we do for the rest of the paper) that the problem of modeling the propagation of the detonation shock and the motion of the reacted products in the following flow is completely described by a solution to the compressible Euler equations for a reactive flow, with a specified equation of state for the explosive and reaction rate of the form

$$e = e(p, v, \lambda), \quad r = r(p, v, \lambda).$$

Here p, v, λ are the pressure, the specific volume, and the progress variable of chemical reaction. When $\lambda = 0$ the explosive is unreacted; $\lambda = 1$ corresponds to a completely reacted explosive.

Prediction of the detonation dynamics can be achieved by direct numerical solution (DNS) of the Euler equations. In order to obtain a highly accurate solution to the reactive Euler equations that will calcuate the detonation speed to 5% or less, it is essential to have enough points in the reaction zone. In our own studies [9], we showed that as many as 20–100 cells in the streamwise direction are required for sufficient accuracy for engineering calculations. When one considers the consequences of such a fine scale for the reaction zone, combined with the requirement for global temporal and spatial accuracy in the meter-sized domain of the engineering device, huge computational resources are required, even with current TeraFlop parallel computing resources.

The computational barrier to three-dimensional (3D) design of explosive systems by direct solution of the reactive Euler equations is not newly discovered and dates back to WWII when one of the first uses of computers was explosive design. The barrier presents a dilemma for modelers. One needs to make predictions in engineering systems but one cannot overcome the huge computational requirements and associated costs needed to compute on the device scale. (One *can* carry out adequately resolved DNS of the reactive Euler equations on scales that are least two orders of magnitude smaller than the system scale.) The difficulty, posed by trying to solve a physically correct but computationally intractable model for an explosive system, is similar to the prediction of incompressible turbulence on engineering device scales by direct numerical solution of the Navier–Stokes equations. Turbulence modeling of flows on larger engineering-device scales has led to the development of subscale models for turbulence and most recently to large eddy simulation. The computational requirements for large-eddy simulations are orders of magnitude less than those required for direct solution of the Navier–Stokes equation.

For the computation of detonation systems, an attack on the dilemma has led to the invention of subscale models for the propagating detonation front that we refer to herein as

program burn (PB) models. The program burn model does *not* try to resolve the fine scale of the reaction zone in the sense of a DNS simulation. The program burn simulation (PBS) does try to solve for the flow in the inert product gases on a grid that is too coarse to resolve the physical reaction zone of the reactive Euler equations. Instead, a PBS deposits a prescribed amount of energy (and more generally mass and momentum) into a *very small* number of computational cells behind a shock front with precalculated motion. The effective reaction zone in a PBS is a region where source terms are added to account for the deposition of energy, and it is always behind the location of the precalculated shock front. To get the advantages of simulation with lower computational requirements, the effective reaction zone is always constrained to be a finite number of cells thick (between 1 and 8, but much less than 20, say).

As the grid is refined and the cell thickness goes to zero, the region where the source terms make their contribution is limited to a sharp front with zero thickness across which there are jumps in the dependent state variables. The program burn source doses historically have been prescribed only by peculiar, discrete algorithms used in particular codes. Necessarily, these discrete algorithms must be limited to partial differential equations for the inert compressible Euler equation with delta function sources centered at the location of the sharp front. The front is then externally prescribed by a precalculation of the shock motion. The delta function source terms, represented in the partial differential equations along with the shock motion specification, define the program burn model independent of its discretization and the numerical algorithms that might be used to solve it. One thing is clear from this discussion: the solutions of the reactive Euler equations *are not* solutions of the equations of the program burn model.

In this paper we consider the following problem: How does one make consistent and robust discrete approximations of physical detonation flows with a finite length reaction zone as modeled by the reactive Euler equations, with a discrete approximation to a program burn model that has the reaction zone and shock collapsed entirely to a single discontinuous front?

If we want to design a PB model that has solutions that are in some sense close to those of the Euler equations for a reactive flow, then the quality of the predictions will depend on the accuray of the shock dynamics that are used as input in the precalculation of the shock motion. If we use an approximation to the shock motion, then the accuracy of approximate theory in regard to the shock dynamics is paramount. This issue must be decided irrespective of numerics. Detonation shock dynamics (DSD), developed by a collaboration of the authors Bdzil and Stewart [3, 4], is an asymptotic theory based on a large radius of curvature of the shock relative to the reaction zone length and it has been used succesfully to compute detonation shock motion. A compendium of results of DSD can be found in the review paper [5].

In Section 2 we briefly present direct numerical simulations of the reactive Euler equations that are to be used as the benchmark calculations for the rest of the paper. The geometry considered is planar, cylindrical, or spherical. For both cylindrical and spherical geometry, curvature of the lead shock is present. In Section 3 we compare the solutions obtained from DNS to those obtained from DSD. In Section 4 we discuss a traditional pressure-based program burn (TPB) model. Section 5 presents modified models aimed at improving the weaknesses inherent in the TPB model, especially when curvature is present. This new class of models will be referred to as modified pressure-based program burn models (MPB). The essential difference between TPB and MPB is that TPB uses a Huygen's construction for

the shock propagation rule (shock propagates with the Chapman–Jouguet speed), while if curvature is present, MPB uses a propagation rule based on DSD. Finally, conclusions are given in Section 6. We also note that in the mid-1990s Bdzil and Stewart modified major TPB codes at Los Alamos National Laboratory to include curvature dependence using DSD theory. Also, systematic comparisons were made between TPB models and DNS simulations and their work was not published at that time. To our knowledge this is the first discussion of these models and is a partial record of our earlier work.

2. DIRECT NUMERICAL SIMULATIONS

Here we present the reactive Euler equations whose solutions are used to compare with those of the program burn models presented in subsequent sections. We take the DNS calculations to be "exact" and assume that any differences in solution structure are due to the various definitions and approximations inherent in the program burn models themselves.

For the DNS calculations, the conservative formulation of the reactive Euler equations is given by

$$\vec{U}_t + \vec{F}_x = \vec{G} + \vec{q}r, \tag{1}$$

where

$$\vec{U} = [\rho, \rho u, E, \rho\lambda]^T, \tag{2}$$

$$\vec{F} = [\rho u, \rho u^2 + p, u(E + p), \rho u\lambda]^T, \tag{3}$$

$$\vec{G} = -\frac{j}{x}[\rho u, \rho u^2, u(E + p), \rho u\lambda]^T, \quad \vec{q} = [0, 0, 0, 1]^T, \tag{4}$$

where ρ is the density, p the pressure, u the velocity, and E the total energy, defined by

$$E = \rho\left(e + \frac{1}{2}u^2\right). \tag{5}$$

The specific internal energy is e, and λ is the mass fraction of the deficient component with $\lambda = 0$ for unreacted material and $\lambda = 1$ for completely reacted material. The geometric source terms from the flow divergence are represented explicitly by $\vec{G}$. The choice of j determines the geometry; $j = 0$ for planar, $j = 1$ for cylindrical, or $j = 2$ for spherical geometry. If one assumes a cylindrical/spherical shock, the shock total curvature κ is related to the radius x from the center of the coordinate system by $\kappa = j/x$.

The explosive is described by the constitutive forms for the energy and rate laws. For this paper our baseline example of a condensed phase explosive is that considered in [9] and used as a test problem in [6, 7]. The equation of state is for an ideal gas

$$e = \frac{1}{\gamma - 1}\frac{p}{\rho} - Q\lambda, \tag{6}$$

where γ is the ratio of specific heats and Q is the heat of reaction for the detonation. The reaction rate is given by

$$r = k(1 - \lambda)^{1/2}. \tag{7}$$

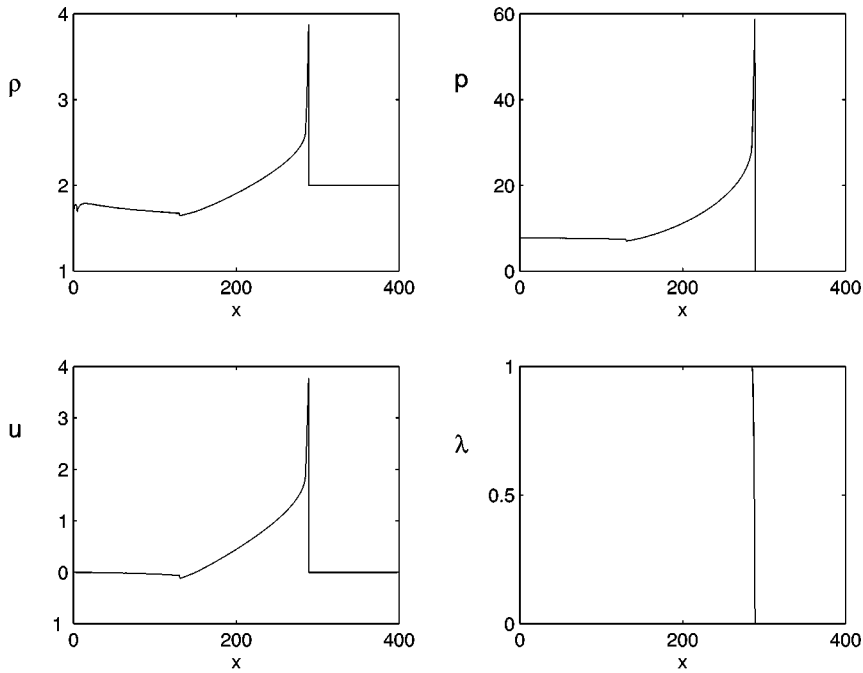

FIG. 1. Plot of the structure for the case $j = 1$ (cylindrical) at time $t = 40$ μs.

The values $Q = 4$ mm$^2/\mu$s^2 and $\gamma = 3$ are taken, with upstream conditions $p_0 = 0$, $\rho_0 = 2$ g/cm^3, $u_0 = 0$, and $k = 2.5147$ μs^{-1}. These values give a Chapman–Jouguet detonation speed of $D_{\mathrm{CJ}} = 8$ mm/μs, and a steady state one-dimensional reaction zone length of 4 mm.

To carry out the DNS, these equations are solved with a third-order TVD Runge–Kutta scheme with a fifth-order WENO spatial scheme [10, 11, 14]. The grid is uniform with $\Delta x = 0.1$ mm, which puts roughly 40 grid points in the reaction zone. Results for 80 grid points in the reaction zone are essentially the same. In all cases, the CFL number was taken to be 0.4. Figures 1 and 2 show wave structures for the case of the case of cylindrical and spherical geometry, respectively. For all the figures shown in the paper, the density unit is g/cm^3, the pressure scale is GPa, the velocity scale is mm/μs, the length scale is mm, and the curvature scale is mm^{-1}.

3. DSD ASYMPTOTIC THEORY AND COMPARISON TO DNS

In this section we briefly state the asymptotic theory of detonation shock dynamic theory, a key ingredient of the program burn model that is presented in subsequent sections. We compare certain flow features between DSD theory and the DNS calculations of the reactive Euler equations presented in the previous section.

3.1. DSD Theory

DSD theory is an asymptotic theory which describes the motion of the detonation shock via an intrinsic partial differential equation that relates the normal shock velocity D_n,

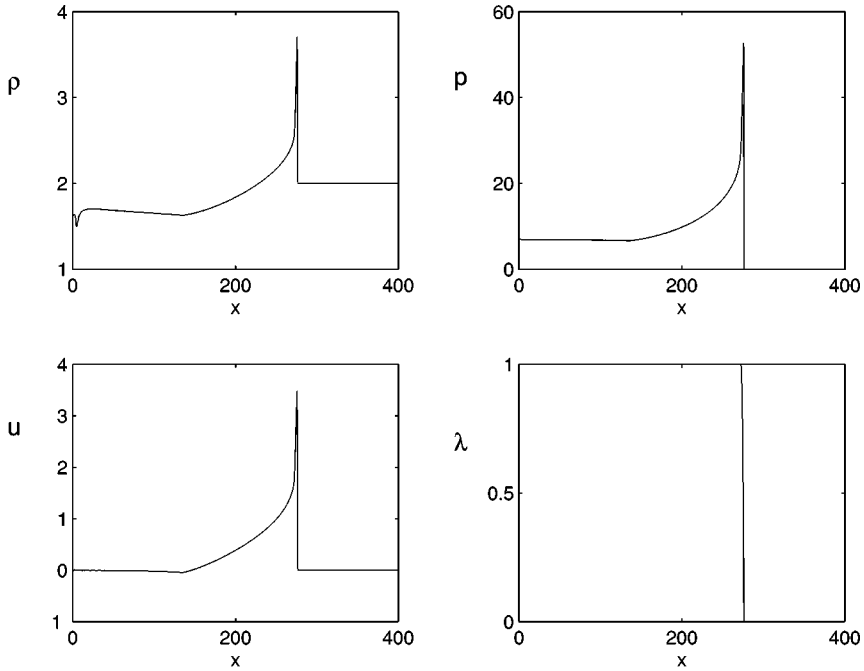

FIG. 2. Plot of the structure for the case $j = 2$ (spherical) at time $t = 40$ μs.

the shock curvature κ, and their time derivatives [5]. For our purposes we focus on the simplest version of DSD that relates the normal shock velocity D_n to the curvature. The relevant equations, consistent with an asymptotic truncation of the reactive Euler equations (presented in a nearly integrable form), are

$$\frac{\partial(\rho U_n)}{\partial n} + \kappa\rho(U_n + D_n) = 0, \tag{8}$$

$$\frac{\partial\left(\rho U_n^2 + p\right)}{\partial n} + \kappa\rho U_n(U_n + D_n) = 0, \tag{9}$$

$$\frac{\partial}{\partial n}\left(e + pv + \frac{1}{2}U_n^2\right) = 0, \tag{10}$$

$$\frac{\partial\lambda}{\partial n} = -\frac{1}{U_n}(r), \tag{11}$$

where n is the coordinate normal to the detonation front, and $U_n = u_n - D_n$ is the relative normal velocity in the shock-attached frame.

An alternative form of the energy equation, dubbed the *master equation*, is found by using the chain rule on $e(p, \rho, \lambda)$ in (10), using the mass equation to substitute for the spatial derivative of ρ, and then using the momentum equation to substitute for the spatial derivative of the pressure p. With the standard definition of the sound speed for an ideal equation of state (EOS), $c^2 = \gamma p/\rho$, one obtains

$$\left(c^2 - U_n^2\right)\frac{\partial U_n}{\partial n} = Qr(\gamma - 1) - \kappa c^2(U_n + D_n). \tag{12}$$

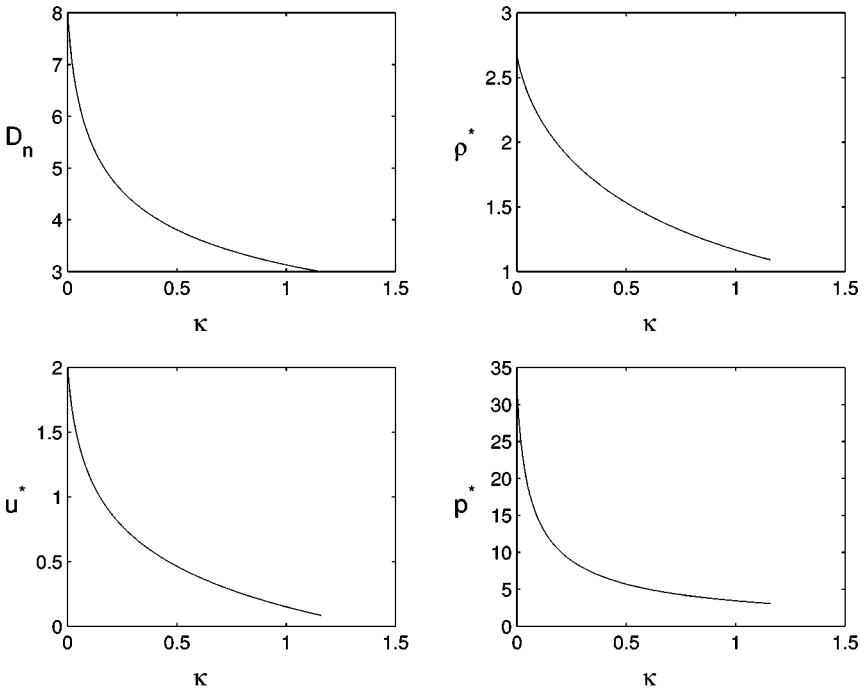

FIG. 3. Plot of the shock speed D_n and the sonic ($*$) states as a function of κ.

The *generalized CJ conditions* follow from the master equation. When the flow is locally sonic with

$$\eta \equiv c^2 - U_n^2 = 0, \tag{13}$$

and the velocity gradient is finite, it follows that the right-hand side of (12) must also be zero; i.e.,

$$\Phi \equiv Qr(\gamma - 1) - \kappa c^2(U_n + D_n) = 0. \tag{14}$$

The first condition is the *sonic condition*, while the second is the *thermicity condition.* These conditions hold for detonations that travel near or at the CJ detonation velocity. The simultaneous mandates that the sonic and thermicity conditions be satisfied mandates a relationship between κ and D_n. For such solutions one can find the sonic, or star ($*$), states. The solution of this nonlinear eigenvalue problem can be done numerically if desired and the sonic states can be found as a function of the local curvature κ. A plot of the sonic states is shown in Fig. 3 for the condensed phase example of the previous section. Note that for $\kappa = 0$, the sonic states are the CJ states, and $D_n = D_{\mathrm{CJ}}$.

3.2. DSD–DNS Comparisons

Comparisons of DSD theory with DNS have been carried out for the cases of detonation along a two-dimensional rate stick, in a converging channel, and in a diverging

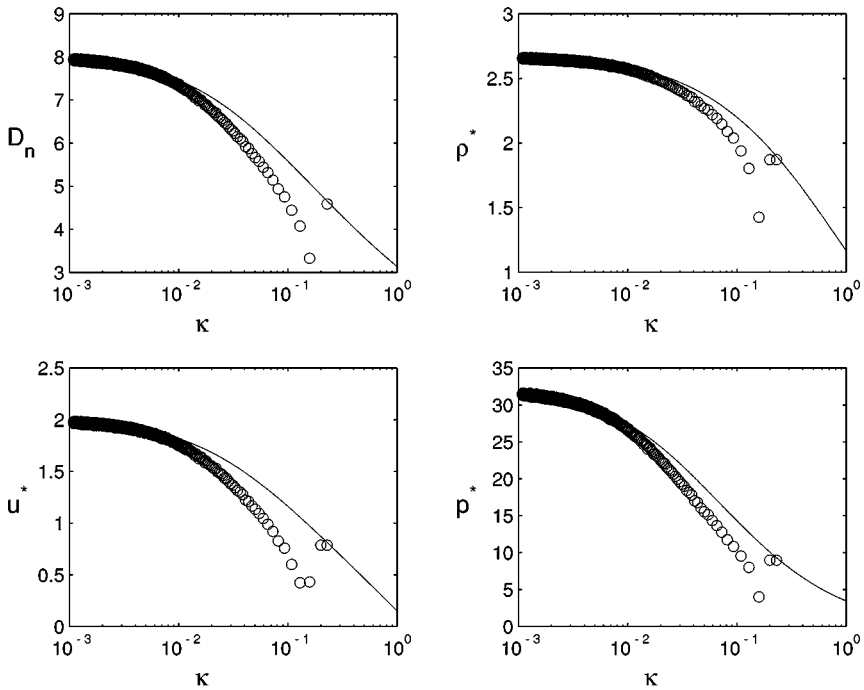

FIG. 4. Plot of D_n and the sonic ($*$) states as a function of κ for DSD (solid) and DNS (circles). Cylindrical geometry.

channel [6]. In all three cases, the shock front locations as computed from DSD theory and from DNS were compared and good agreement between the two was found. Similar comparisons can be found in [7, 8]. However, a simple and direct comparison between DSD and DNS can be carried out by considering cylindrical or spherical geometry where the curvature is explicitly known and the equations are essentially one-dimensional.

Figures 4 and 5 show a comparison of the shock velocity versus curvature and the sonic states calculated from the DNS of the Euler equation, and that predicted from DSD theory for cylindrical and spherical geometry, respectively. In each figure, the solid curve corresponds to DSD theory, and the circles correspond to the DNS calculations. The wave front was determined to be at the location where λ was 0.1. The shock speed was computed from a numerical difference of the shock locations. Note the good agreement for both cylindrical and spherical geometries as the curvature goes to zero, i.e., the long-time solution. For large values of the curvature, the agreement between the two diverge, either due to the transient effects of the DNS calculations at the earlier times or due to the first-order and quasi-steady approximation of DSD theory, where the time derivatives have been ignored.

4. TRADITIONALLY IMPLEMENTED PROGRAM BURN MODELS

Here we discuss the basic ideas behind the implementation of program burn as it has traditionally been implemented in design hydrocodes used for explosive engineering. Although several versions exist, we shall discuss only one model, the traditional pressure-based

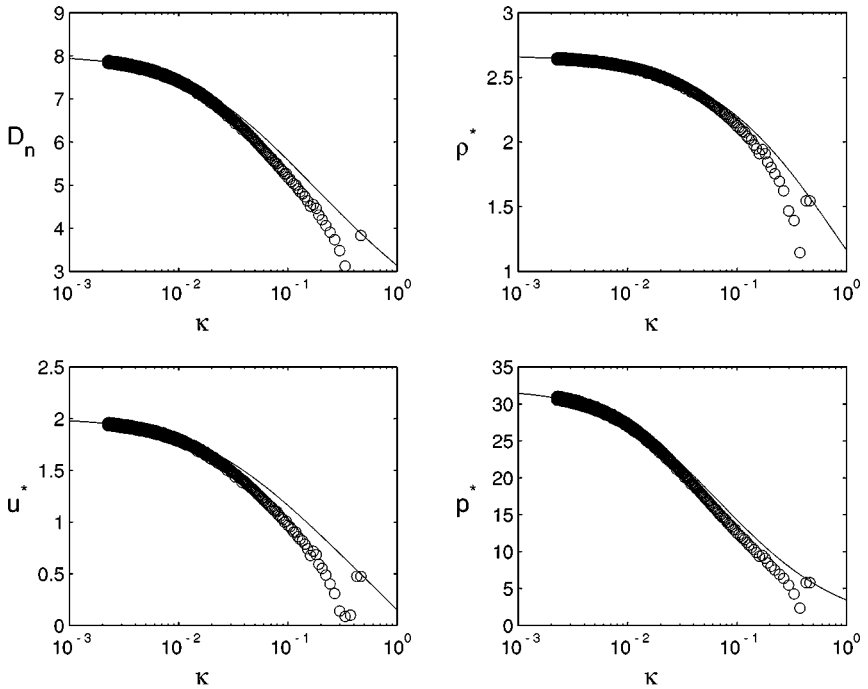

FIG. 5. Plot of D_n and the sonic ($*$) states as a function of κ for DSD (solid) and DNS (circles). Spherical geometry.

program burn model. The other models have similar strengths and weaknesses, and one model is sufficient for our discussion.

As a computational model, program burn was first posed as a discrete numerical algorithm and not in terms of a differential formulation. One of the earliest published references to an algorithm of this type is found in [13]. The algorithm has the following ingredients: (i) There are a predetermined, computational grid and a chosen algorithm for the inert hydrodynamics. The grid defines the domain of the explosive and the algorithms are used to solve the Euler equations for the (inert) explosive products. (ii) A graded set of "burn times," t_b, are assigned to each computational cell on the grid. The burn times are the times at which the detonation shock front crosses the coordinates of the initial position of the computational cell. The traditional way to compute the burn times is to select the unreacted explosive geometry, pick the locus of an initial Chapman–Jouguet (CJ) detonation, and then compute the motion of the detonation shock emanating from the initial locus by means of a Huygens construction. The Huygens construction propagates the shock normal to itself at the constant CJ wave speed, D_{CJ}. (iii) A cell-based algorithm either adds energy to designated burning cells or modifies the equation of state in cells during the interval of the shock passage over the cells, as dictated by the precalculated burn times. The equation of state adjustment has been done in various ways through increments in either the pressure or the specific volume, hence the variations referred to earlier.

In what follows, we give a description of a traditional pressure-based program burn algorithm which modifies the equation of state in the burning cells. The definitions of the burn fraction, the burn time field, precalculated shock motion, and modification of the equation of state are key ingredients of the model.

4.0. Definitions

4.0.1. *Burn Fraction*

Based on a previously calculated assignment, each cell is assigned a burn time, t_b. If the current time of a cell is below the burn time, $t < t_b$, then the cell is not burning and the burn fraction Y is assigned zero. If $t > t_b$, then the burn fraction must be calculated. The burn fraction is usually assigned to be the volume fraction of the undisturbed cell that has been crossed by the detonation shock at that time and hence has a computed value, $0 < Y < 1$. The details of the burn fraction assignment depend on the grid and specific algorithm and whether the burn times are stored at cell centers or at the nodes. If the whole cell has been crossed, the burn fraction is simply $Y = 1$.

4.0.2. *Burn-Time Field*

Once the burn-fraction algorithm is selected, the discrete field of burn fraction can be precalculated from the discrete field of burn times. While (as the grid is resolved) the burn times are limited to a piecewise continuous field in the domain of the unshocked explosive, the discrete burn-fraction field must limit to a singular Heaviside function which is attached to the contours of the burn-time field (i.e., the precalculated shock position). The burn time field is precalculated with a Huygens construction. Thus, once the unreacted explosive geometry is selected and the initial locus of an initial CJ detonation is picked, the motion of the detonation shock that emanates from the initial locus is computed by means of a Huygens construction.

4.0.3. *Shock Surface Motion and the Limits of Discrete Fields*

The way to express these ideas mathematically is as follows. Let the burn-time field be a piecewise continuous field with a discrete representation on a grid which covers the domain of the unreacted explosive, given by

$$t_b(\vec{x}). \tag{15}$$

Then at a fixed time t_0, the shock locations are the contours of the burn-time field

$$t_0 = t_b(\vec{x}_s), \quad \text{for } \vec{x} = \vec{x}_s. \tag{16}$$

The limit of the discrete burn-fraction field at a time t_0 as the mesh is resolved is represented by the Heaviside function

$$H[(\vec{x} - \vec{x}_s(t_0)) \times \hat{n}], \tag{17}$$

where $\hat{n}$ is the normal to the shock that points in the direction of propagation.

As an example, consider a one-dimensional detonation wave propagating with constant positive speed D_{CJ}. Then, according to Huygens's construction, we have

$$\frac{dx_s}{dt} = D_{\mathrm{CJ}}, \tag{18}$$

where x_s is the location of the detonation front at time t. Integrating we get the motion rule for the front

$$x_s(t) = x_0 + t D_{\mathrm{CJ}}, \tag{19}$$

where x_0 is the initial position. The domain $x < x_0$ is assumed to be completely reacted, and is unreacted for $x > x_0$. This relationship can be inverted to yield the burn-time field

$$t_b(x_s) = \frac{x_s - x_0}{D_{\mathrm{CJ}}}. \tag{20}$$

For the discrete approximation, let the numerical grid have a uniform mesh, x_i, with grid spacing Δx. Then the discrete version of the burn field can be written as

$$t_b(x_i) = \frac{x_i - x_0}{D_{\mathrm{CJ}}}, \quad \text{for } x_i > x_0. \tag{21}$$

Note that the burn time is not defined for $x_i \le x_0$, which indicates that this region of the flow field has already reacted. Also note that the burn time is piecewise continuous in the unreacted domain.

For the prescription of the burn-fraction, which we shall denote by Y_i, we update Y_i according to the rule

$$Y_i = \begin{cases} 0 & x_i > x_s, \\ \frac{x_s - x_i}{\Delta x} & x_s - \Delta x < x_i < x_s, \\ 1 & x_i < x_s - \Delta x. \end{cases} \tag{22}$$

This particular description of the burn fraction is defined over a single cell. In the limit as $\Delta x \to 0$, we see that the burn fraction approaches a Heaviside function. Figure 6 shows a sketch of the shock position as a function of time and a sketch of the burn fraction Y, distributed over two cells. The use of the burn fraction Y is described in more detail in the following section.

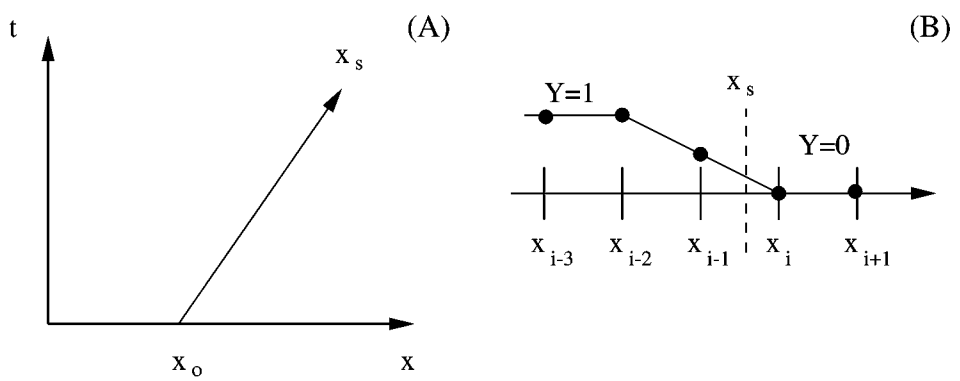

FIG. 6. (A) Sketch of the shock location $x_s(t)$ as a function of time. (B) Sketch of the burn fraction Y on a discrete grid.

4.0.4. *Modification of the Equation of State and Apparent Weak Detonation Structure*

In the traditional pressure-based program burn algorithm one assumes an equation of state for the inert products

$$e_{\text{products}}(p, v) \equiv e(p, v).$$

Since condensed explosives are being considered, the initial pressures (one bar) are extremely small compared to the detonation pressures behind the lead shock (hundreds of kilobars) such that the pressure ahead of the shock in the unreacted explosive can be considered to be zero. This is similar to the strong shock approximation. In a PBS, the burning cells where the burn-fraction Y is between 0 and 1, the equation of state is modified by replacing p with p/Y to obtain $e_{\text{products}}(p/Y, v)$. This is equivalent to replacing the pressure with a partial pressure which is reduced by the burn-fraction for that cell. When $Y = 1$, the equation of state for the products is recovered. Finally, in the unburnt cells in the unreacted explosive one must give an energy that is consistent with the heat of detonation. This is done in the following way. One considers the standard Rankine–Hugoniot relations for a gasdynamic discontinuity for a steady Chapman–Jouguet discontinuity traveling at laboratory speed D_{CJ}. One then sets the energy datum e_0 in the unreacted explosive consistent with that algebra. The equation of state for TPB can thus be written as

$$e = e_0 \times (1 - H[(\vec{x} - \vec{x}_s(t)) \times \hat{n}]) + e_{\text{products}}(p/Y, v) \times H[(\vec{x} - \vec{x}_s(t)) \times \hat{n}]. \quad (23)$$

An example of selecting e_0 is presented in the following section.

If we consider the pressure variation across the shock during a PB, the pressure starts out from zero and is brought up to a high value near the CJ pressure. Indeed, when the burn fraction Y is zero, the pressure is necessarily assumed to be zero. In fact, the scheme computes the pressure and is based on an assumed equation of state. Therefore, the underlying hydrodynamic algorithm must increment the pressure in such a way that the internal energy is assumed to be *finite*. A simple conclusion is that the effective reaction zone structure of traditional program burn starts at the unreacted state at the ambient pressure, and *not* at the shock state. If the program burn algorithm can be interpreted in terms of an effective distributed rate law, then the corresponding detonation structure looks like a weak detonation, and not a strong detonation. Note that the physically based argument that a weak detonation needs a supersonic trigger to start the chemical reaction is absent in a PBS, since the precalculated shock motion provides the sequenced burn-times for the cells that trigger the change in the equation of state in the vicinity of the shock. An alternative interpretation is that the PB scheme is a capturing scheme which intends to capture states that are near or at the steady state equilibrium CJ values. Hence, the physical reaction zone structure from the inert unreacted shock state (the von Neumann spike) to the sonic point that normally would be computed as part of the reaction zone in a DNS is cut off and not represented.

4.1. Example: Ideal EOS

To illustrate the traditional implementation of program burn, we will start with an ideal EOS for the detonation products, $e(p, v)$

$$e(p, v) = \frac{1}{\gamma - 1}\frac{p}{\rho}.$$

4.1.1. *CJ States*

To compute the CJ states, we first assume that the unburnt upstream state (with the strong shock approximation) ahead of the wave is given by

$$\rho = \rho_0, \quad u = 0, \quad p = 0, \quad e = e_0, \tag{24}$$

with e_0 unspecified at this point (but to be chosen in the course of the analysis). Let $[\,] = (\,)_0 - (\,)_b$ denote the jump in a quantity across the interface from the 0-state ($Y = 0$) to the completely burnt state ($Y = 1$) denoted by a b subscript. The normal jump conditions across the interface moving with speed D_n are given by

$$[\rho(u_n - D_n)] = 0, \tag{25}$$

$$[\rho u_n(u_n - D_n) + p] = 0, \tag{26}$$

$$[E(u_n - D_n) + u_n p] = 0, \tag{27}$$

where E is the total energy defined earlier. With the ideal EOS for the burnt products, the jump condition algebra derives a quadratic equation for the normal particle velocity u_n, say. If we identify the speed D_n as the CJ value (D_{CJ}), the quadratic equation for u_n can be solved to give

$$u_n = \frac{D_{\mathrm{CJ}} \pm \sqrt{D_{\mathrm{CJ}}^2 - 2(\gamma^2 - 1)e_0}}{\gamma + 1}. \tag{28}$$

The CJ-state is found by setting with the zero of the argument of the radical equal to zero, which leads to the identification of either the D_{CJ} in terms of the energy e_0 or vice versa. Since we generally regard D_{CJ} as being given experimentally, we choose to write the condition as

$$e_0 = \frac{D_{\mathrm{CJ}}^2}{2(\gamma^2 - 1)}. \tag{29}$$

Then the CJ-states are

$$\rho_{\mathrm{CJ}} = \rho_0\left(\frac{\gamma + 1}{\gamma}\right), \quad p_{\mathrm{CJ}} = \frac{\rho_0 D_{\mathrm{CJ}}^2}{\gamma + 1}, \quad u_{\mathrm{CJ}} = \frac{D_{\mathrm{CJ}}}{\gamma + 1}. \tag{30}$$

It also follows simply that the CJ-state is locally sonic. Note that in working out the Rankine–Hugoniot jump conditions across a program burn discontinuity, from the unreacted explosive to the burnt explosive where the burn fraction Y is set equal to one, one obtains exactly the same Rankine–Hugoniot algebra as the reactive Euler equation where λ is set equal to one. Thus, the variation of a burn-fraction variable has no effect on the calculation of the CJ-states themselves.

As an example, we take the condensed phase explosive found in [9]. With $\gamma = 3$, $\rho_0 = 2$ g/cc, and $D_{\mathrm{CJ}} = 8\,\mathrm{mm}/\mu\mathrm{s}$, we get for the CJ-states

$$\rho_{\mathrm{CJ}} = \frac{8}{3}\ \mathrm{g/cc}, \quad p_{\mathrm{CJ}} = 32\ \mathrm{GPa}, \quad u_{\mathrm{CJ}} = 2\ \mathrm{mm}/\mu\mathrm{s}. \tag{31}$$

4.1.2. *Equation of State with Modified Pressure and Effects on the Structure*

In keeping with the notion that one replaces p with p/Y in the burning cells with $0 < Y \leq 1$, the ideal EOS becomes

$$e = \frac{1}{\gamma - 1}\frac{p}{Y\rho}. \tag{32}$$

Again one assumes that in the fresh material one has the same initial specific internal energy e_0, and the role of e_0 is the same as the heat of detonation.

To further analyze this structure, let $U_n = u_n - D_n$ be the relative normal velocity in the shock-attached frame. For a quasi-steady traveling wave, the RH relations hold throughout the structure, except now the internal energy has the dependence on the burn fraction Y. As before, one can again solve the RH relations

$$\rho U_n = -\rho_0 D_n \tag{33}$$

$$\rho U_n^2 + p = \rho_0 D_n^2 \tag{34}$$

$$e + \frac{1}{2}U_n^2 + \frac{p}{\rho} = e_0 + \frac{1}{2}D_n^2, \quad \text{with } e = \frac{p}{\rho Y(\gamma - 1)}, \tag{35}$$

for a quadratic equation in U_n with solutions

$$U_n = -\frac{[1 + (\gamma - 1)Y]D_n \pm \sqrt{D_n^2 - 2(\gamma - 1)Y[2 + (\gamma - 1)Y]e_0}}{2 + (\gamma - 1)Y}. \tag{36}$$

When $Y = 0$, the plus root corresponds to the unreacted flow state, and hence to the starting point for a weak detonation structure,

$$U_n = -D_n, \quad \text{or} \quad u_n = 0. \tag{37}$$

The root associated with the minus sign is pathological and has $U_n = 0$ or $u_n = D_n$, and corresponds to a finite pressure but infinite density. In contrast, the standard strong shock state $U_n = -(\gamma - 1)/(\gamma + 1)D_n$ is achieved if the equation of state $e = pv/(\gamma - 1)$ is used instead of the modified equation of state $e = (p/Y)v/(\gamma - 1)$.

The issue is which state is selected, and we turn to the acoustic character of the distributed structure next. From the fundamental definition of the sound speed,

$$c^2 = \frac{p/\rho^2 - \partial e/\partial \rho}{\partial e/\partial p},$$

we have

$$c^2 = \frac{p}{\rho}[1 + (\gamma - 1)Y].$$

Next, if we use the energy equation $e + p/\rho + U_n^2/2 = D_n^2/2 + e_0$ and use the definitions of e and the last result for c^2, we can eliminate p/ρ in favor of c and write an expression for the sonic parameter, η, as

$$\eta \equiv c^2 - U_n^2 = \left[e_0 + \frac{1}{2}\left(D_n^2 - U_n^2\right)\right](\gamma - 1)Y - U_n^2.$$

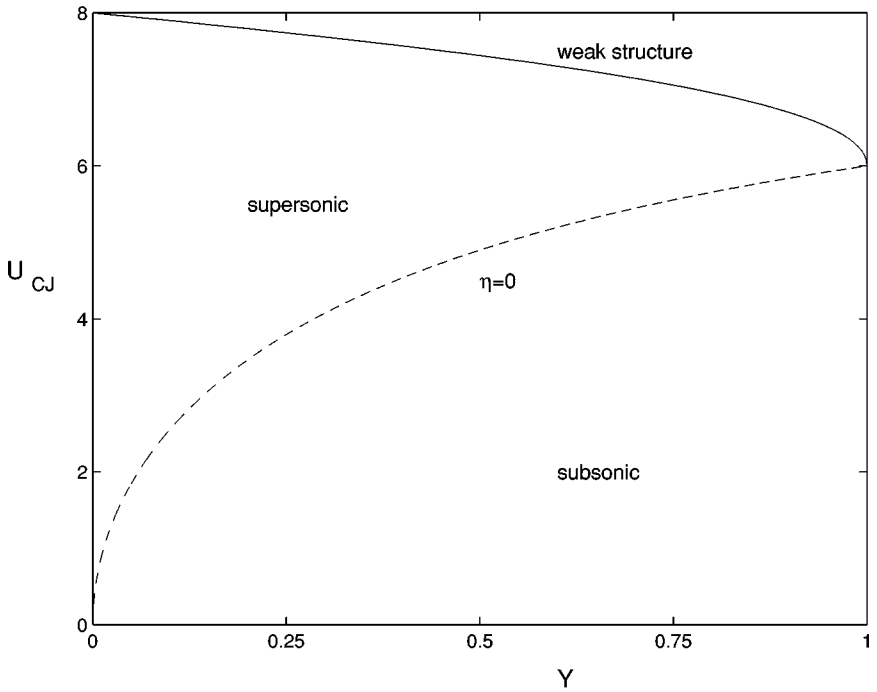

FIG. 7. U_{CJ}, Y-plane showing the trajectory of the weak CJ detonation. The dash curve corresponds to the sonic locus given by (38) and the solid curve corresponds to the weak structure given by (36). (The strong structure branch is not shown.)

If the detonation wave starts out on the weak branch, then at $Y = 0$, $c = 0$, and $U_n = -D_n$, the sonic parameter $\eta = -D_n^2 < 0$, and the wave is supersonic at the point of the lead disturbance. In fact one can compute the sonic locus in a (U_n^2, Y)-plane by setting $c^2 = U_n^2$ to obtain

$$U_n^2 = \frac{\gamma^2(\gamma - 1)e_0 Y}{[1 + 1/2(\gamma - 1)Y]}. \tag{38}$$

The character of the structure of the (weak) detonation can be characterized by plotting its trajectory in a (U_n, Y)-plane. The weak CJ solution trajectory starts from the undisturbed state, $U_n = -D_n$ and terminates at the sonic state. Figure 7 shows this trajectory for the specific case of $D_n = D_{\mathrm{CJ}}$. Note the square root behavior in U_n as $Y \to 1$, suggesting that the normal derivative has a square root singularity. This is due to the fact that the thermicity condition in the master equation does not vanish at the sonic point.

The other required ingredient for a weak detonation is a supersonic trigger. Ordinarily, the supersonic trigger is regarded as physical. But for its application as a numerical algorithm, program burn assigns times at which the cell releases its energy. Specifically, the value of the burn fraction is changed from $Y = 0$ to $Y = 1$ in proportion to how much of the particle cell has been crossed by an assumed shock wave. Therefore, the distribution of times when the cell is crossed by a shock is known a priori, and is used to create the supersonic trigger. For steady, one-dimensional flow for a CJ detonation, the burn times simply and exactly reflect the CJ detonation velocity.

We note that the state variables do depend on the burn fraction if the burn fraction were distributed in a discrete representation, i.e., not resolved to a Heaviside step function. Thus the burn fraction distribution on a finite mesh has the appearance of a pseudo-reaction-zone structure. We will model this distribution not by a difference-based scheme, but instead by an "effective" rate law in the steady detonation frame,

$$U_n \frac{\partial Y}{\partial n} = R(Y), \tag{39}$$

where $R(Y)$ is the effective reaction rate. In actual practice this rate is not given at all, rather the numerical scheme that defines the burn fraction merely makes an assignment for the increase in Y such that it goes to $Y = 1$ when the detonation shock crosses the computational cell completely, and $R(Y)$ is inferred from the details of that assignment. But certainly $R(Y)$ is both grid- and algorithm-dependent.

Integration of (39), with the weak-structure relation between U_n and Y and the condition that $Y = 0$ at $x = 0$ (which is equivalent to the specification of the triggering event at the program burn time), leads to a distribution function $Y(x)$ which has the basic profile shown in Fig. 6.

An important observation is that the thickness of the heat-release zone in the program burn reaction zone will be a function of the grid thickness and can be computed asymptotically as $O(\Delta x)$, such that as $\Delta x \to 0$, the program burn reaction zone vanishes, as measured relative to *any* physical length scale. Thus, the effect of the numerical algorithm that $R(Y)$ imitates is to approximate a delta function, centered at the burn times and locations on the grid as dictated by the burn table.

4.2. Numerical Results of TPB and Comparisons to DNS

Here we present numerical results comparing the solutions obtained using the traditional pressure-based program burn model (TPB) to the solutions obtained from a DNS calculation that is desribed in Section 2. For the TPB model we solve the corresponding nonreactive Euler equations with the EOS given by (23) and (29). Although most TPB implementation in current codes use a second-order scheme, we use the same (high-order) scheme that was used for the DNS calculations to minimize differences that may result from the use of different numerical algorithms. To restate, we assume that the DNS calculations are "exact," and that any differences in solution structure will be due to the various approximations inherent in the TPB model.

A mesh with one grid point in the reaction zone ($\Delta x = 2\,\text{mm}$) is used that is typical of that used in engineering practice. No attempt is made here to optimize nor study the effect of grid spacing on the solution structures. However, the grid is fine enough to resolve the inert hydrodynamics behind the wave front.

Figure 8 shows the results from the DNS (solid) and from the TPB (circles) calculations for planar geometry. (Note that the density spike shown in the DNS record is associated with the initial start-up transient.) In each case, the solutions were stopped when the shock location reached $x_s(t) = 100$ mm. The arrival times of the two calculations is seen to be approximately the same (for DNS, $t = 12.72\,\mu$s; for TPB, $t = 12.05\,\mu$s), the 5% relative difference being due to differences in the grid resolutions and to the modeling assumptions of the reaction zone by the TPB model. Note how well the program burn model captures the overall structure. The only differences are seen in the density plot, where the DNS

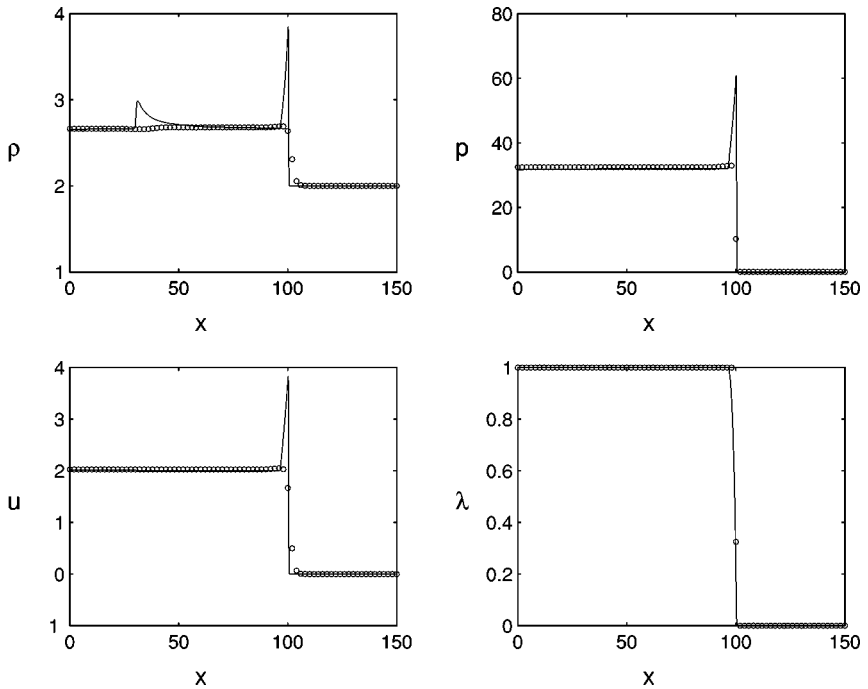

FIG. 8. Plot of the structure for planar geometry at $x_s(t) = 100\,\text{mm}$. Circles correspond to the TPB model ($t = 12.05\,\mu\text{s}$), and the solid curve to DNS ($t = 12.72\,\mu\text{s}$).

calculates a weak density jump downstream of the lead shock while the TPB calculations (with the coarser grid) do not, and in the lead shock region, where the DNS calculations show a strong detonation profile while the TPB calculations show a weak detonation profile. We also ran long-time solutions until the shock was located at $x_s(t) = 900\,\text{mm}$, as shown in Fig. 9. The arrival times of the two calculations have a relative difference of less than 1% (for DNS, $t = 112.77\,\mu\text{s}$; for TPB, $t = 111.97\,\mu\text{s}$). Again, note how well the program burn model captures the overall structure.

The major weakness of the TPB model, however, occurs when curvature is present. Figure 10 shows the structure from the DNS and from the TPB calculations for the case of cylindrical geometry. Since the TPB uses a Huygens construction to propagate the shock, we see that the arrival time of the shock to the location $x_s = 100\,\text{mm}$ is much quicker ($t = 12.075\,\mu\text{s}$) than that of the DNS calculations ($t = 15.3\,\mu\text{s}$); this represents roughly a 21% error in the arrival times. This large difference is not due to grid resolution, but rather to the TPB modeling of the shock speed using a Huygens construction. Since Huygens's construction overestimates the speed of the shock when curvature is present, we see noticeable differences in the solution structures downstream of the lead shock. We also ran long-time solutions for the cylindrical and spherical cases, until the shock was located at $x_s(t) = 900\,\text{mm}$ as shown in Fig. 11. A close-up look at the structure is shown in Fig. 12.

In terms of the structure, the program burn model does seem to capture the overall structure at the longer times rather well. A closer look at the time behavior can be examined by comparing the shock speed and the sonic states to those obtained from DSD theory (see Fig. 13). Note that the TPB-calculated shock velocity overpredicts the DSD-calculated velocity, and that the sonic states are only asymptotic to the sonic states obtained from DSD theory.

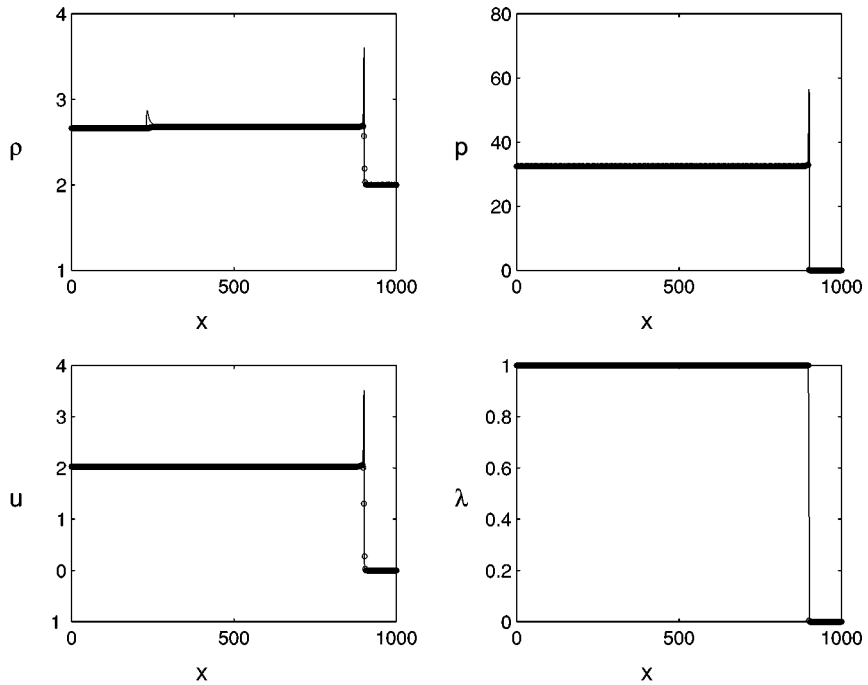

FIG. 9. Plot of the structure for planar geometry at $x_s(t) = 900\,\text{mm}$. Circles correspond to the TPB model ($t = 111.97\,\mu\text{s}$), and the solid curve to DNS ($t = 112.77\,\mu\text{s}$).

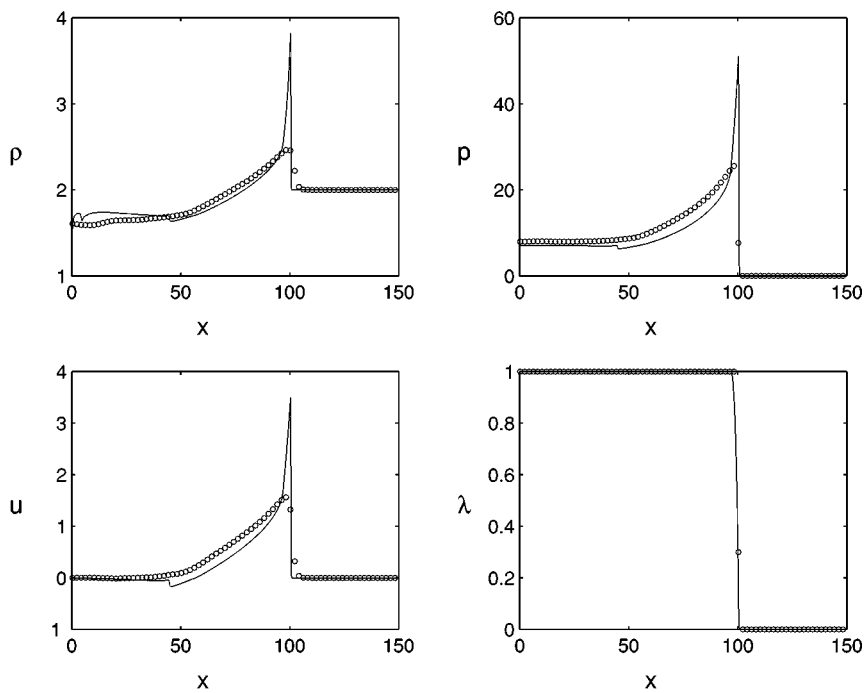

FIG. 10. Plot of the structure for cylindrical geometry at $x_s(t) = 100\,\text{mm}$. Circles correspond to the TPB model ($t = 12.075\,\mu\text{s}$), and the solid curve to DNS ($t = 15.3\,\mu\text{s}$).

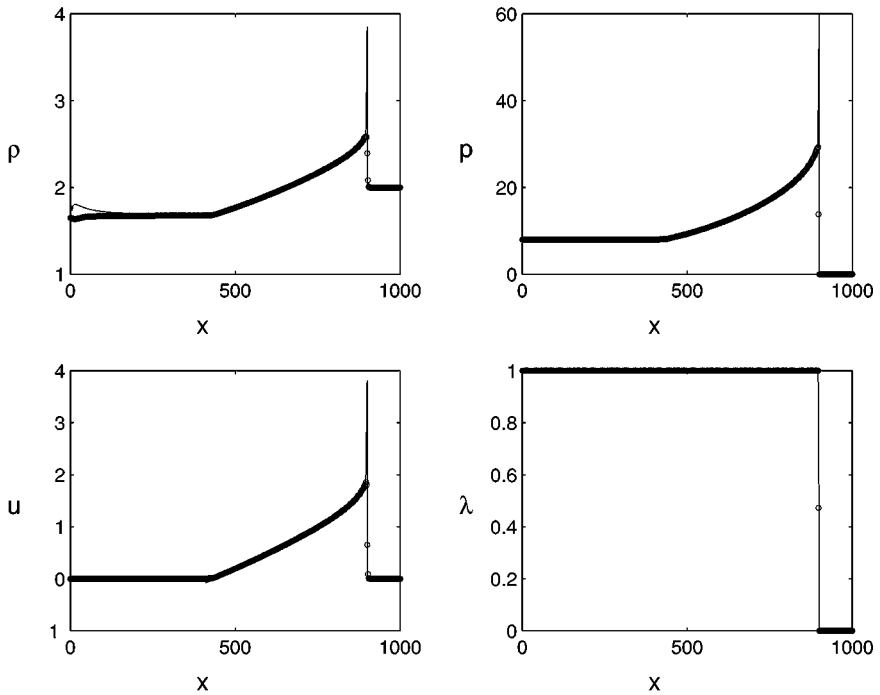

FIG. 11. Plot of the structure for cylindrical geometry at $x_s(t) = 900\,\text{mm}$. Circles correspond to the TPB model ($t = 112.0\,\mu\text{s}$), and the solid curve to DNS ($t = 117.6\,\mu\text{s}$).

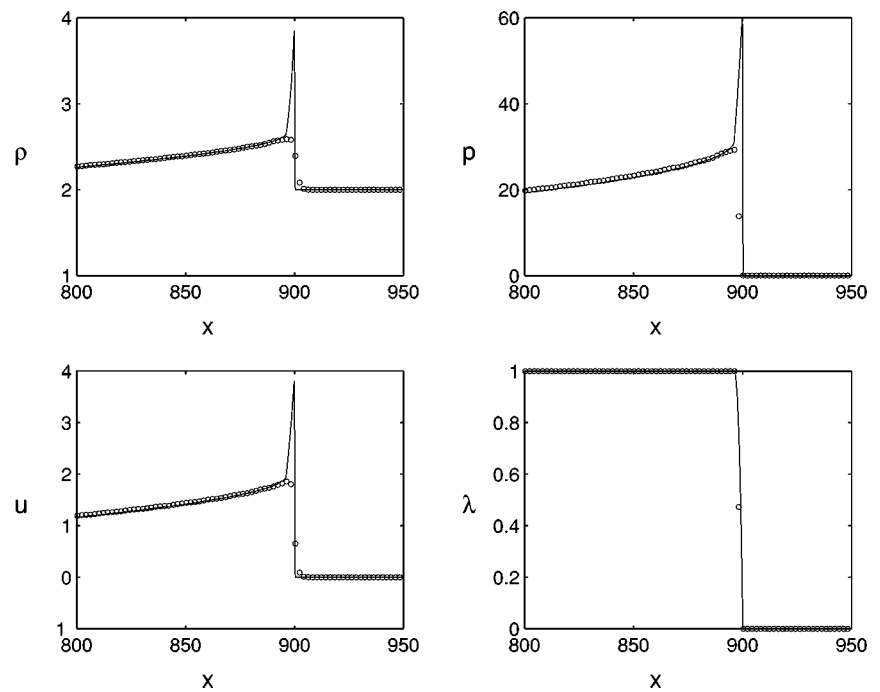

FIG. 12. Blow-up of the shock structure shown in Fig. 12 for cylindrical geometry at $x_s(t) = 900\,\text{mm}$. Circles correspond to the TPB model ($t = 112.0\,\mu\text{s}$), and the solid curve to DNS ($t = 117.6\,\mu\text{s}$).

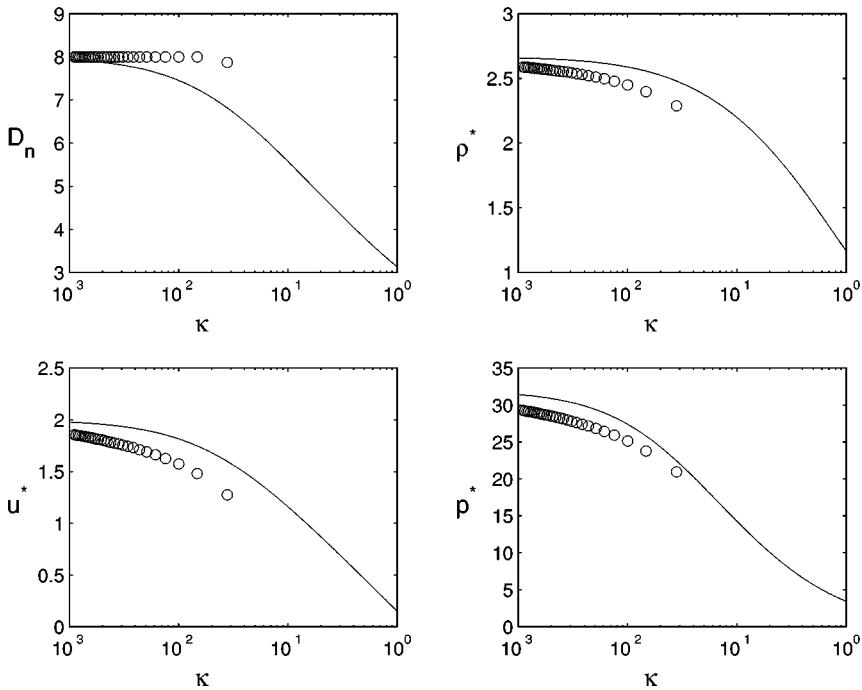

FIG. 13. Plot of D_n and the sonic ($*$) states as a function of κ for DSD (solid) and TPB (circles).

The above results illustrates the strength and weaknesses of using the traditional program burn model to capture the physics of real detonations. For the planar case, the shock is propagated at the correct CJ speed, and the structure is represented well with only $1/40$th the number of grid points. This represents significant computational savings. However, when curvature is present there are major differences in not only the shock location but also in the structure of the solution. These differences are due to the fact that Huygens's construction overestimates the speed of the propagating shock. Since curvature is present in almost all engineering devices, it is essential to properly take into account effects due to curvature. It is this weakness that we address in the subsequent section of this paper.

5. MODIFIED PRESSURE-BASED PROGRAM BURN MODELS

In the previous section we have seen that when curvature is present, the TPB model overestimates the detonation shock speed, due to the use of Huygens's construction. This leads to significant differences of the shock location and to a lesser extent to differences in the structure between the DNS and the TPB simulations. A simple modification can be made by extending the theory to include curvature dependent shock velocity, as is found in DSD theory. In particular, we modify the burn times to include the curvature dependence

$$\frac{dx_s}{dt} = D_n(\kappa), \tag{40}$$

and compute D_n according to DSD theory, for a particular equation of state. Having done this the next question is what is the best way to model the physical reaction zone? Next,

we present four models that aim at being improvements to the TPB model, especially when shock curvature is present.

5.1. Model I or MPB-1

In this model we modify the upstream internal energy to account for curvature effects, namely

$$e_0 = \frac{D_n^2}{2(\gamma^2 - 1)}, \tag{41}$$

where $D_n = D_n(\kappa)$ is the curvature-dependent shock velocity determined from DSD theory. This program burn model is composed of modification of the burn times according to (40) and the assignment of the explosive upstream energy according to (41).

Figure 14 shows a comparison of results of the DNS and MPB-1 for cylindrical geometry. Note that a simple change in the way the burn times are computed and in the definition of the upstream internal energy can lead to significant reductions in differences between the two. As for the case of comparison between the TPB and DNS, the simulations were stopped when the shock location reached $x_s(t) = 100$ mm. The arrival times of the shock for the MPB-1 and DNS is seen to be approximately the same (for DNS, $t = 15.3\,\mu$s; for MPB-1, $t = 14.2\,\mu$s), and the 7% relative time of arrival difference is a major improvement when compared to the 21% relative time of arrival difference in the arrival times found in comparing the TPB and DNS. Comparing Figures 10 and 14, we see that the MPB-1 does a

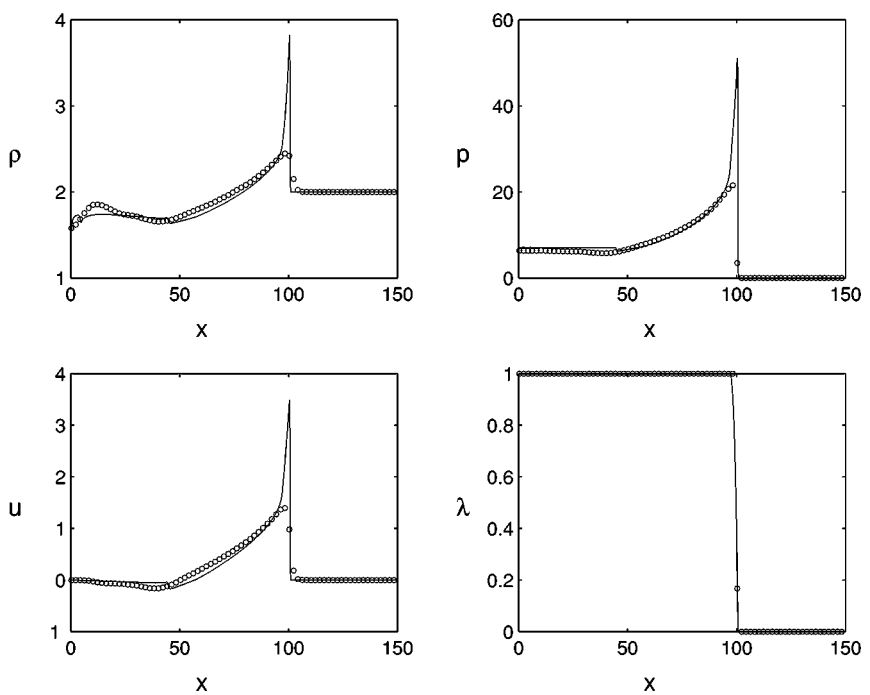

FIG. 14. Plot of the structure for cylindrical geometry with $\Delta x = 2$ mm at $x_s(t) = 100$ mm. Circles correspond to the MPB-1 ($t = 14.2\,\mu$s), and the solid curve to DNS ($t = 15.3\,\mu$s).

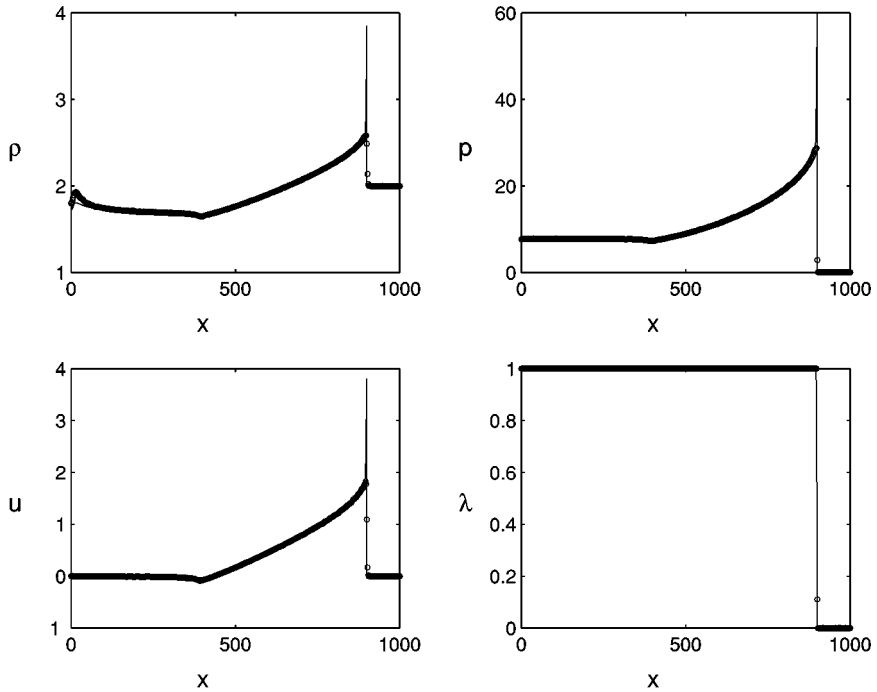

FIG. 15. Plot of the structure for cylindrical geometry with $\Delta x = 2\,\text{mm}$ at $x_s(t) = 900\,\text{mm}$. Circles correspond to the MPB-1 ($t = 116.76\,\mu\text{s}$), and the solid curve to DNS ($t = 117.6\,\mu\text{s}$).

better job of capturing the pressure and velocity profiles than does the TPB model. The long time solution, when $x_s(t) = 900\,\text{mm}$, is shown in Figs. 15 and 16, and should be compared to Figs. 11 and 12, for the TPB model.

However, MPB-1 fails to capture the correct sonic (or $*$) states. Capturing the correct sonic states is an important indicator of how well a given scheme does since both the strong detonation and the weak detonation should terminate at this point. In Fig. 17 we plot the sonic states as computed from the MPB-1 simulations against those determined from DSD theory. We take this comparison to indicate that there is still an unacceptably large discrepancy, even though the correct speed dependence on curvature is incorporated into the MPB-1 model. In Fig. 18 the computed sonic states are shown for the grid with $\Delta x = 0.5\,\text{mm}$ and there is better agreement with the DSD sonic states. In these calculations the energy released is still over a single grid point, so reducing Δx reduces the effective reaction zone. Also note that the oscillations in the shock speed D_n observed in Fig. 17 have been reduced by grid resolution. Note that extreme refinement of the MPB-1 model violates the spirit of the program burn model, i.e., that it should be used on a relatively coarse grid, and no further grid refinements are shown here.

5.2. Model II or MPB-2

For model MPB-2 we keep the specification of the upstream internal energy unchanged

$$e_0 = \frac{D_{\text{CJ}}^2}{2(\gamma^2 - 1)}, \tag{42}$$

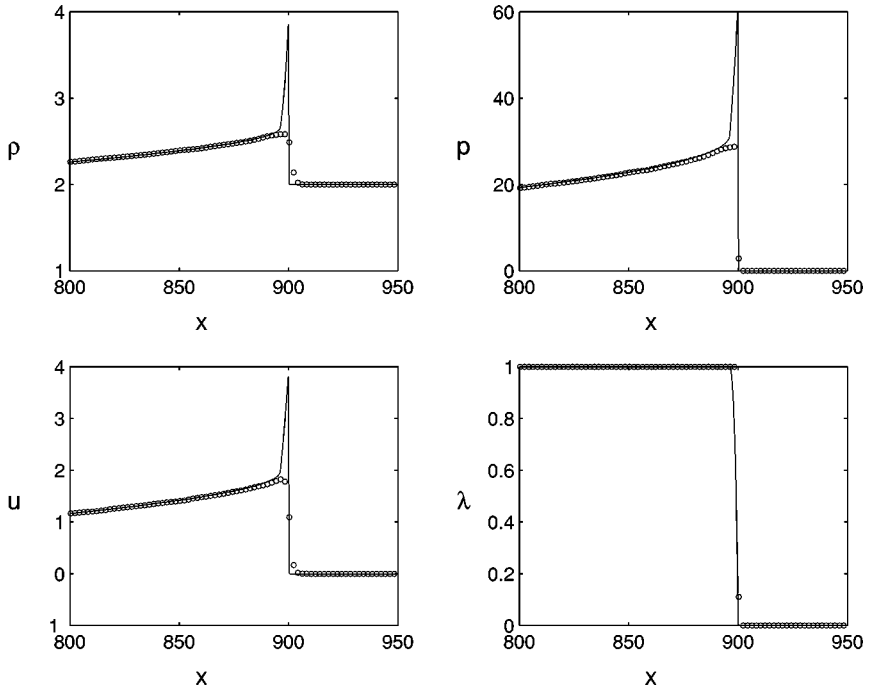

FIG. 16. Blow-up of the shock structure shown in Fig. 15 for cylindrical geometry with $\Delta x = 2\,\text{mm}$ at $x_s(t) = 900\,\text{mm}$.Circles correspond to the MPB-1 ($t = 116.76\,\mu\text{s}$), and the solid curve to DNS ($t = 117.6\,\mu\text{s}$).

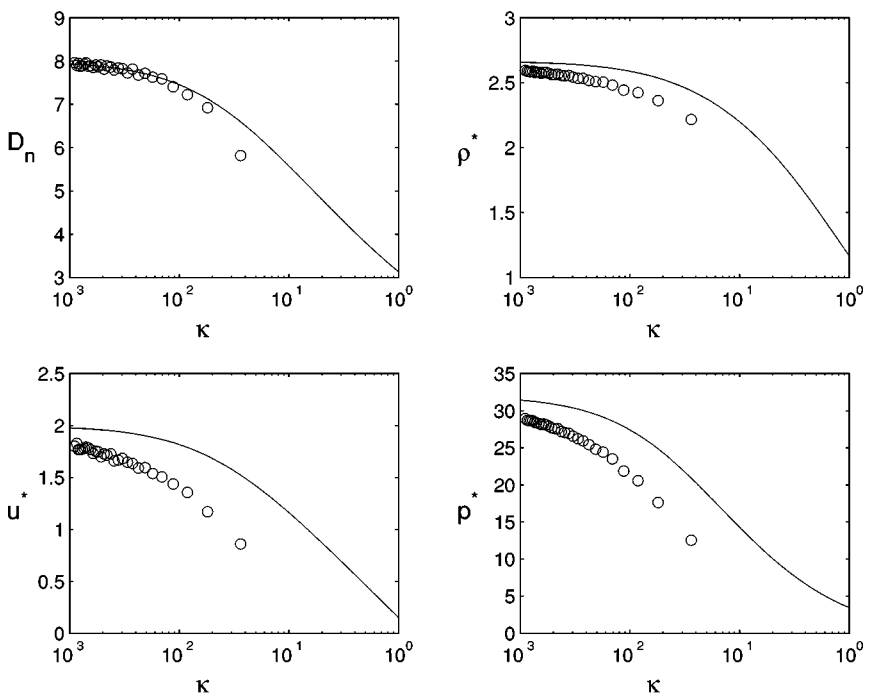

FIG. 17. Plot of D_n and the sonic ($*$) states as a function of κ for DSD (solid) and MPB-1 (circles) with $\Delta x = 2\,\text{mm}$.

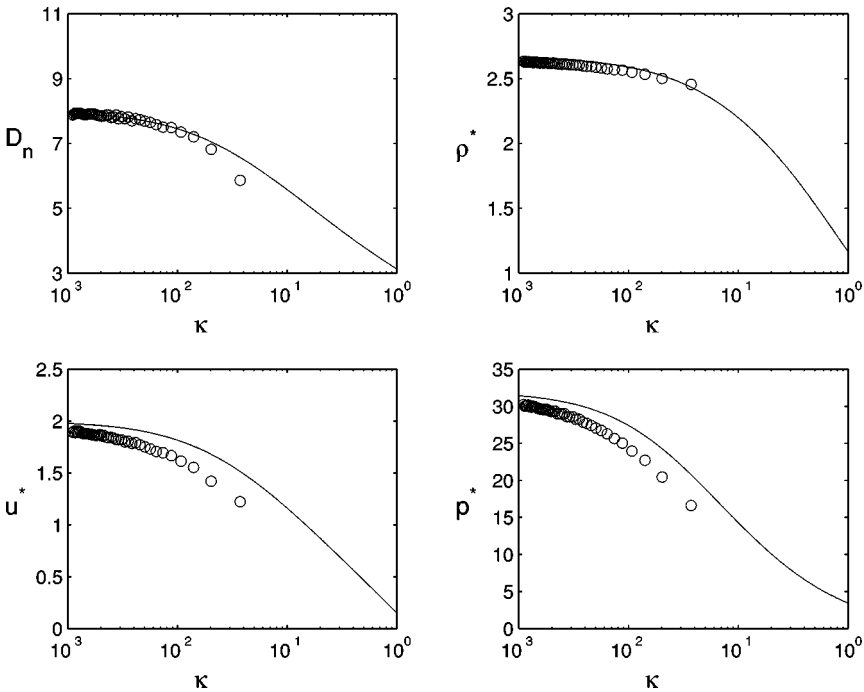

FIG. 18. Plot of D_n and the sonic ($*$) states as a function of κ for DSD (solid) and MPB-1 (circles) with $\Delta x = 0.5\,\text{mm}$.

but modify the length scale of the program burn reaction zone to mimic the reaction zone thickness of the physical problem. Thus, we allow the energy to be released over a number of cells behind the precalculated shock front. However, the resolution of the energy release is still much too coarse to be considered equivalent to that of a resolved DNS. For the TPB model, the program burn reaction zone thickness is kept at one grid cell, independent of grid resolution. Thus, as the grid size becomes smaller, so does the program burn reaction zone thickness. However, for MPB-2 we preassign a program burn reaction zone thickness which has a length scale of approximately the same size as that of the physical (DNS) problem, so that as the grid size becomes smaller, the program burn reaction zone stays fixed and the number of computational cells within it increases. In particular, if L is the program burn reaction zone length, we select the number of computational cells, n, within the zone so that

$$n\Delta x = L. \tag{43}$$

For the DNS example, the 1D Chapman–Jouget reaction zone length is 4 mm. Therefore, for these tests, we set our program burn length $L = 4\,\text{mm}$ for simplicity. Thus, the MPB-2 model consists of using the DSD-based burn-time calculations that are given by the integration of (40), the assignment of the full upstream energy according to (42), and the release of the energy over n-cells according to (43).

Figures 19 and 20 show results for MPB-2 for two different grid resolutions. In Fig. 19, the grid resolution is 2 mm and $n = 2$. Note that the near-shock structure is quite different from that of MPB-1 (compare Fig. 14). For MPB-1, the upstream value of e_0 is reduced

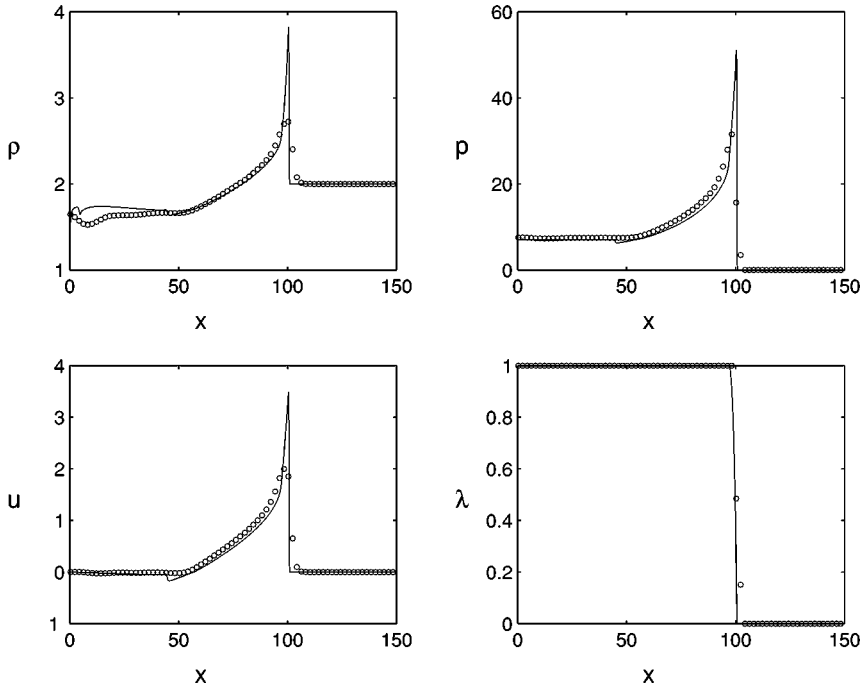

FIG. 19. Plot of the structure for cylindrical geometry with $\Delta x = 2$ mm at $x_s(t) = 100$ mm, with $n = 2$. Circles correspond to the MPB-2 ($t = 14.5\,\mu$s), and the solid curve to DNS ($t = 15.3\,\mu$s).

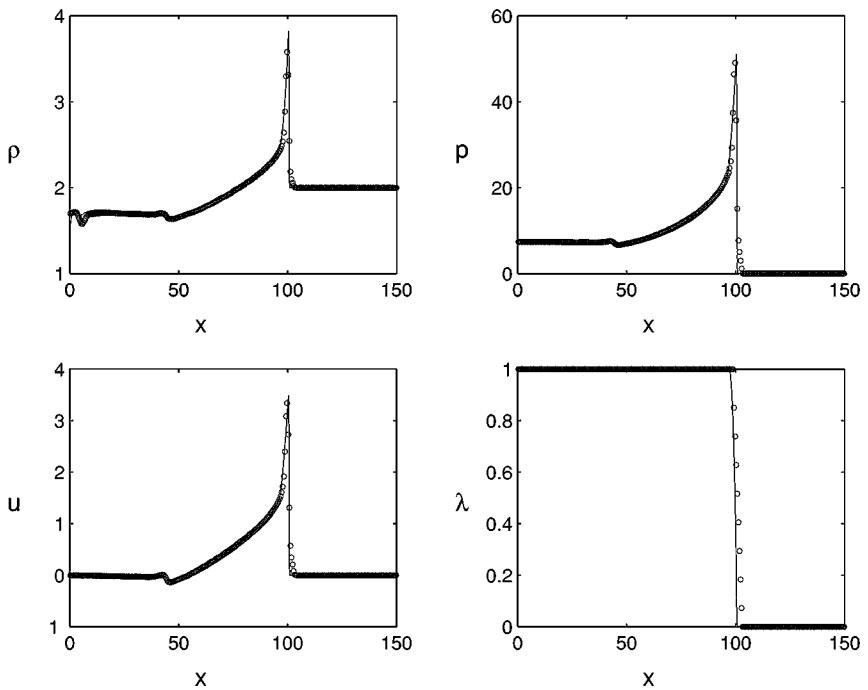

FIG. 20. Plot of the structure for cylindrical geometry with $\Delta x = 0.5$ mm at $x_s(t) = 100$ mm, with $n = 8$. Circles correspond to the MPB-2 ($t = 14.5\,\mu$s), and the solid curve to DNS ($t = 15.3\,\mu$s).

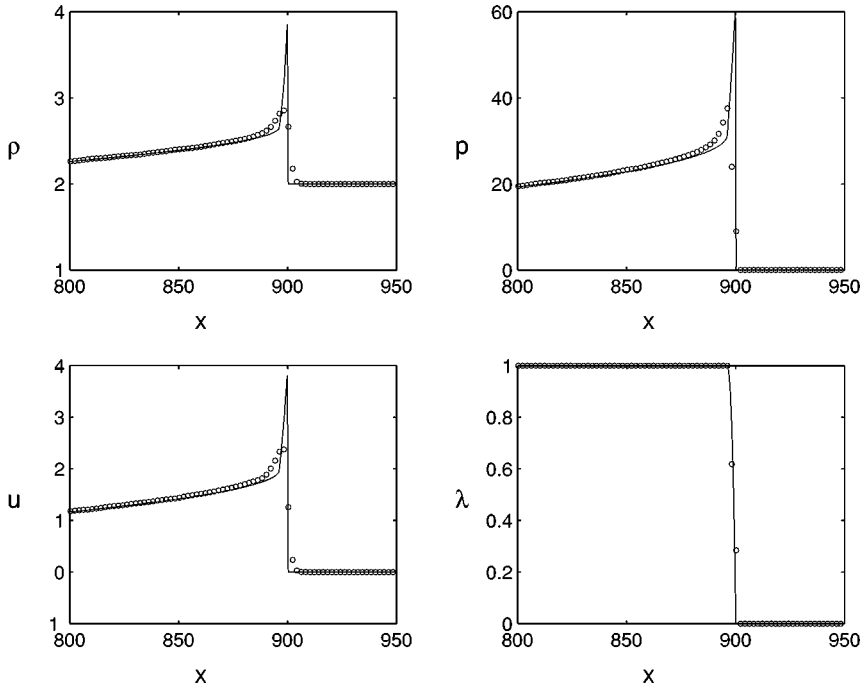

FIG. 21. Plot of the structure for cylindrical geometry with $\Delta x = 2$ mm at $x_s(t) = 900$ mm, with $n = 2$. Circles correspond to the MPB-2 ($t = 117.76$ μs), and the solid curve to DNS ($t = 117.6$ μs).

and depends on curvature through the dependence on D_n and the structure looks like a weak detonation. However, for MPB-2, when e_0 is fixed to be the full explosive energy, the discrete near-shock structure looks like a conventional strong detonation. Decreasing the grid size for MPB-2 to 0.5 mm with $n = 8F$ not only captures the overall flow structure better than the coarse resolution, with $n = 2$, but also does a better job of capturing the near-shock detonation structure. The same is true at the longer times, where we show a blow up of the structure for a grid resolution of 2 mm with $n = 2$ (Fig. 21) and a grid resolution of 0.5 mm with $n = 8$ (Fig. 22). The captured sonic states for MPB-2 are comparable to those shown in Fig. 18, but were found to be noisy and are not shown.

5.3. Model III or MPB-3a and MPB-3b

Here we present results from third model that has two variations that we dubb MPB-3a and MPB-3b. In this case we add mass and momentum source terms, in addition to an energy source term. Models MPB-1 and MPB-2 only added energy source terms. The formulation for MPB-3 are given by the equation

$$\vec{U}_t + \vec{F}_x = \vec{G} + \vec{Q} R_{\delta(x - x_s(t))}, \tag{44}$$

where

$$\vec{U} = [\rho, \rho u, E]^T, \tag{45}$$

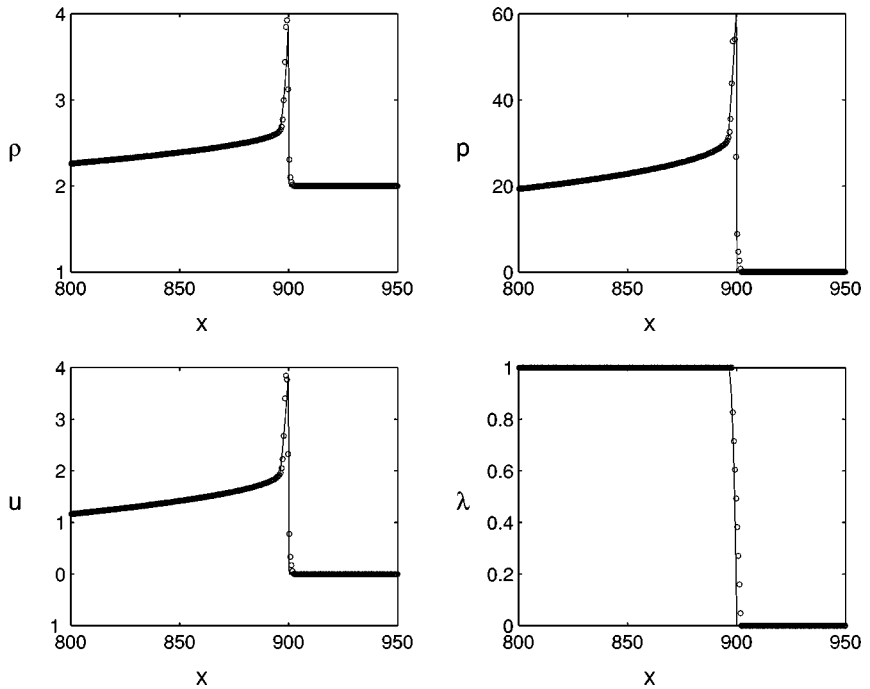

FIG. 22. Plot of the structure for cylindrical geometry with $\Delta x = 0.5$ mm at $x_s(t) = 900$ mm, with $n = 8$. Circles correspond to the MPB-1I ($t = 14.5\ \mu$s), and the solid curve to DNS ($t = 117.6\ \mu$s).

$$\vec{F} = [\rho u,\ \rho u^2 + p,\ u(E + p)]^T, \tag{46}$$

$$\vec{G} = -\frac{j}{x}\,[\rho u,\ \rho u^2,\ (E + p)u]^T, \quad \vec{Q} = [Q_1,\ Q_2,\ Q_3]^T, \tag{47}$$

where E is the total energy $E = \rho(e + \frac{1}{2}u^2)$ and e is the internal energy that is described below. Note that $R_{\delta(x - x_s(t))}$ is a delta function centered on the program shock locus $x = x_s(t)$ and the geometric source term $\vec{G}$ is identical in its first three components of its DNS counterpart. The source strengths $\vec{Q}$ are identified below.

Model MPB-3a uses the same modified EOS as the TPB model,

$$e = \frac{p/Y}{\rho(\gamma - 1)}, \tag{48}$$

and the upstream value of the internal energy, e_0, is given by (41). Model MPB-3b uses the standard equation of state without the burn fraction for the ideal gas

$$e = \frac{p}{\rho(\gamma - 1)}. \tag{49}$$

The upstream value of the internal energy is given by $e_0 = 0$, consistent with the strong shock approximation. To completely specify the program burn PDEs one must identify the source term strength $\vec{Q}$. Various specifications are made and analyzed below. (Alternatively and perhaps more consistently we could have chosen the energy datum to be given by (42).

The explosive's chemical energy is typically assigned to the unreacted solid. But the results do not depend on a specific constant value of the energy datum. For model MPB-3b, $e_0 = 0$ was chosen for simplicity.)

One way to determine values of $\vec{Q}$ is to make the quasi-steady assumption and neglect the explicit dependence of curvature in the program burn equations. The lead shock is taken to be at $x = x_s(t)$ with speed D_n, which can depend on curvature and is given by the D_n, κ relation from DSD theory. Across the shock we allow for doses to the mass, momentum, and energy, and the jump conditions across the program-burn shock are given by

$$[\rho(u_n - D_n)] = Q_1[Y], \tag{50}$$

$$[\rho u_n(u_n - D_n) + p] = Q_2[Y], \tag{51}$$

$$[E(u_n - D_n) + u_n p] = Q_3[Y], \tag{52}$$

where $[\phi] = \phi_0 - \phi^*$, and the sonic states are determined using DSD theory. Note that in writing down these normal jump conditions we assumed that $R_\delta = dY/dn$, where n is the normal coordinate. Since the shock location is known, and both the upstream states and the sonic states are known, the jump relations become formulas for explicit evaluation of the doses $\vec{Q}$.

Evaluating the jumps leads to the following specifications for the components of $\vec{Q}$:

$$\begin{aligned} Q_1 &= \rho_0 D + \rho^*(u^* - D_n), \\ Q_2 &= p^* + \rho^* u^*(u^* - D_n), \\ Q_3 &= \rho_0 e_0 D_n + E^*(u^* - D_n) + u^* p^*. \end{aligned} \tag{53}$$

A plot of the sonic states was given previously in Fig. 3 for the condensed phase explosive example given in [9]. The values of $\vec{Q}$ as computed from these formulas is shown in Fig. 23 for both MPB-3a and MPB-3b, respectively. Results for the two models are given in Figs. 24–27 for MPB-3a and in Figs. 28–31 for MPB-3b. These results are in qualitative agreements with TPB (Model I).

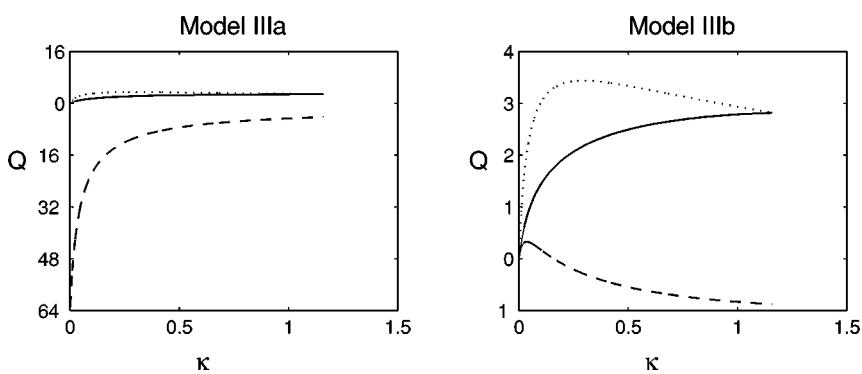

FIG. 23. Plot of Q_1 (solid), Q_2 (dotted), and Q_3 (dashed) as a function of κ for models MPB-3a and MPB-3b, respectively.

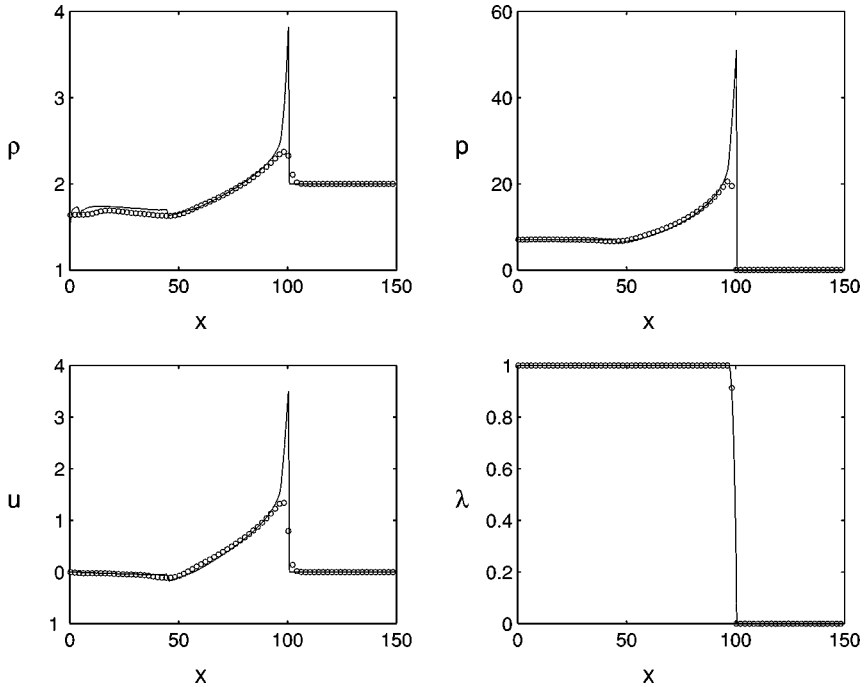

FIG. 24. Plot of the structure for cylindrical geometry with $\Delta x = 2\,\text{mm}$ at $x_s(t) = 100\,\text{mm}$. Circles correspond to the model MPB-3a ($t = 14.2\ \mu\text{s}$), and the solid curve to DNS ($t = 15.3\ \mu\text{s}$).

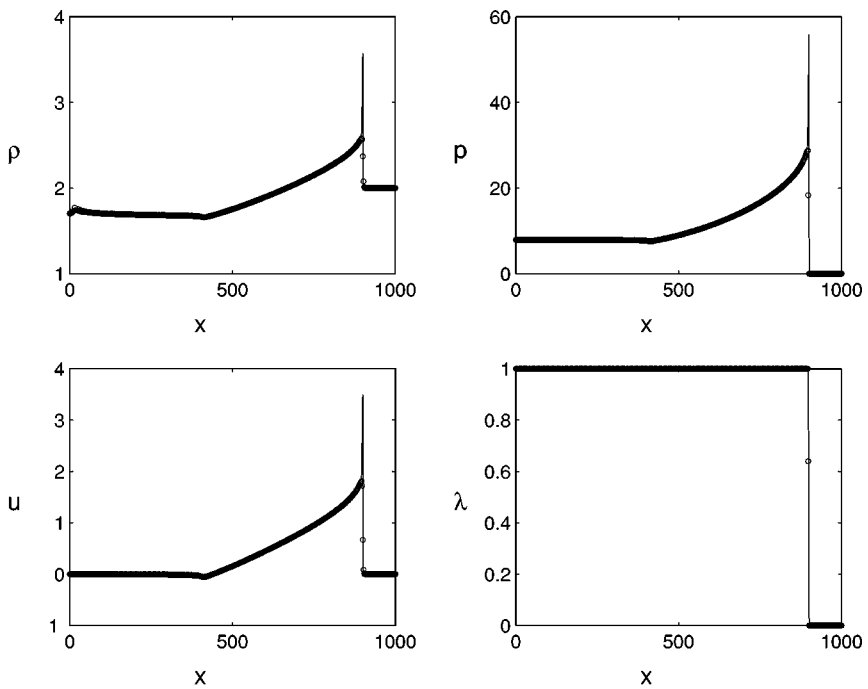

FIG. 25. Plot of the structure for cylindrical geometry with $\Delta x = 2\,\text{mm}$ at $x_s(t) = 900\,\text{mm}$. Circles correspond to the model MPB-3a ($t = 116.2\ \mu\text{s}$), and the solid curve to DNS ($t = 127.5\ \mu\text{s}$).

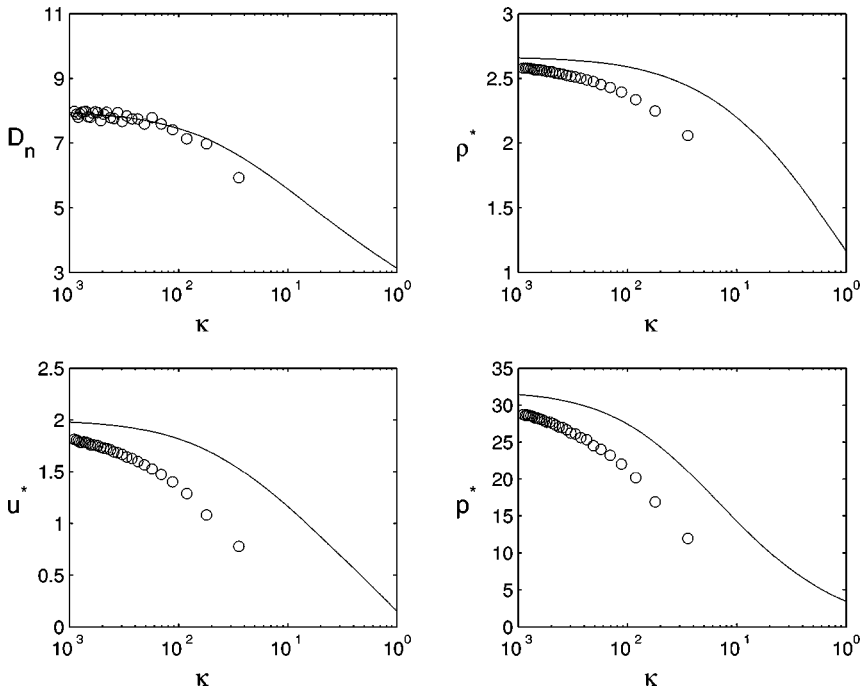

FIG. 26. Plot of D_n and the sonic ($*$) states as a function of κ for DSD (solid) and model MPB-3a (circles) with $\Delta x = 2$ mm.

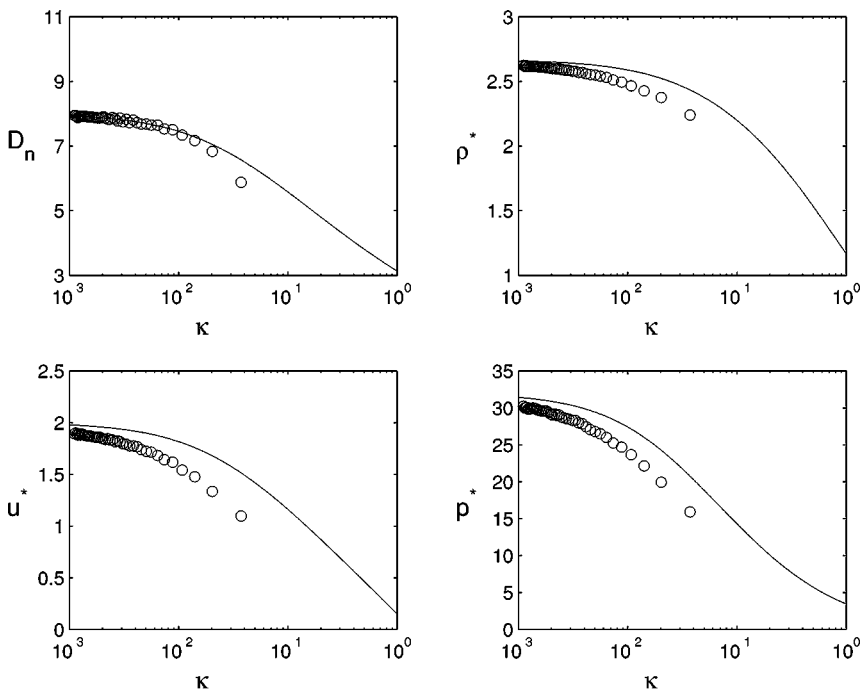

FIG. 27. Plot of D_n and the sonic ($*$) states as a function of κ for DSD (solid) and model MPB-3a (circles) with $\Delta x = 0.5$ mm.

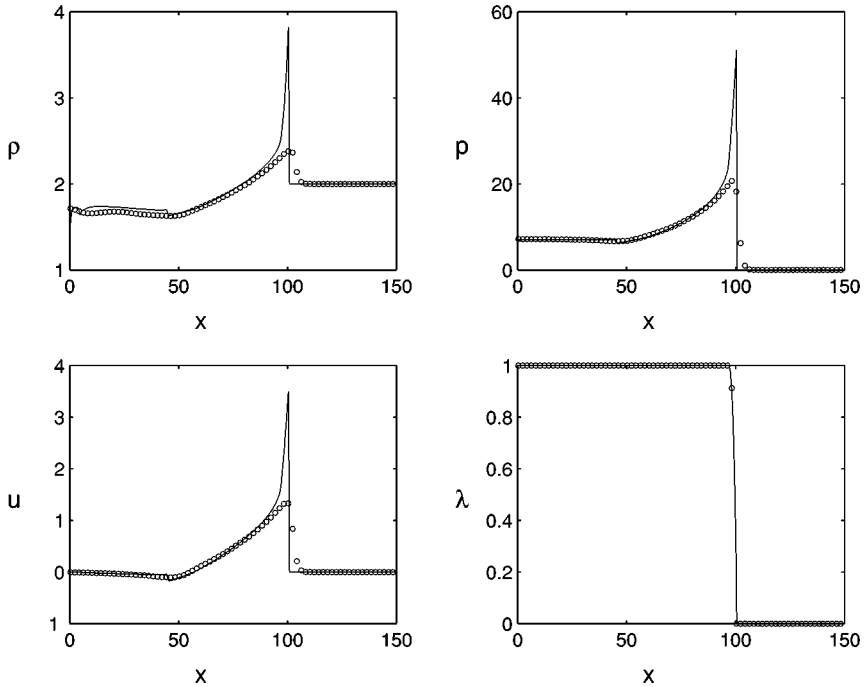

FIG. 28. Plot of the structure for cylindrical geometry with $\Delta x = 2$ mm at $x_s(t) = 100$ mm. Circles correspond to the model MPB-3b ($t = 14.2$ μs), and the solid curve to DNS ($t = 15.3$ μs).

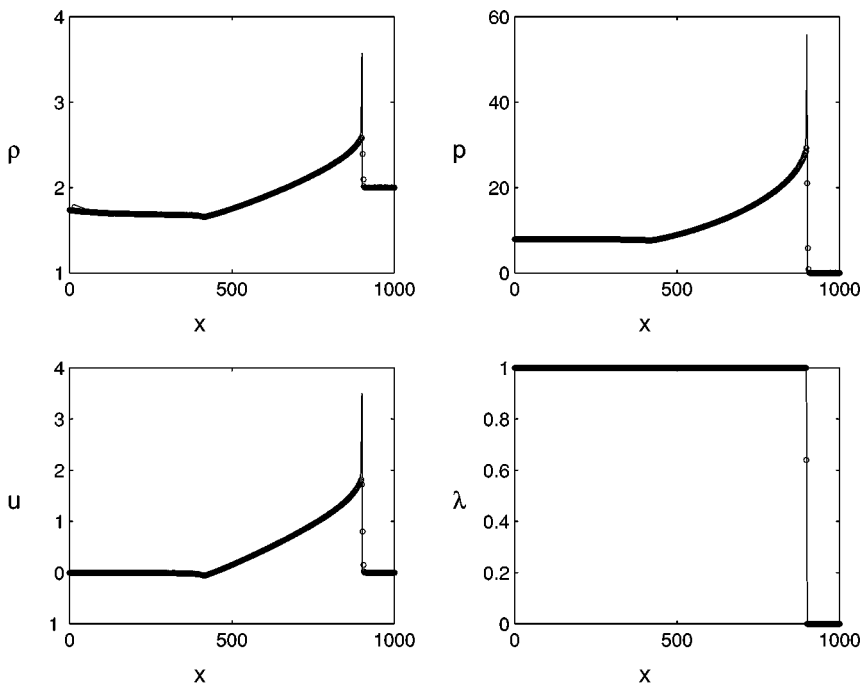

FIG. 29. Plot of the structure for cylindrical geometry with $\Delta x = 2$ mm at $x_s(t) = 900$ mm. Circles correspond to the model MPB-3b ($t = 116.2$ μs), and the solid curve to DNS ($t = 127.5$ μs).

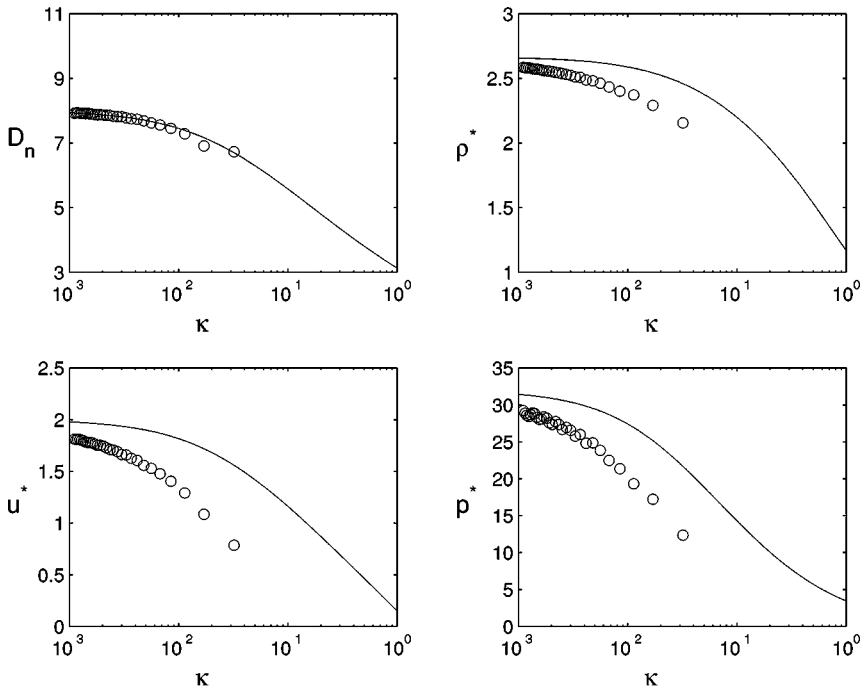

FIG. 30. Plot of D_n and the sonic ($*$) states as a function of κ for DSD (solid) and model MPB-3b (circles) with $\Delta x = 2$ mm.

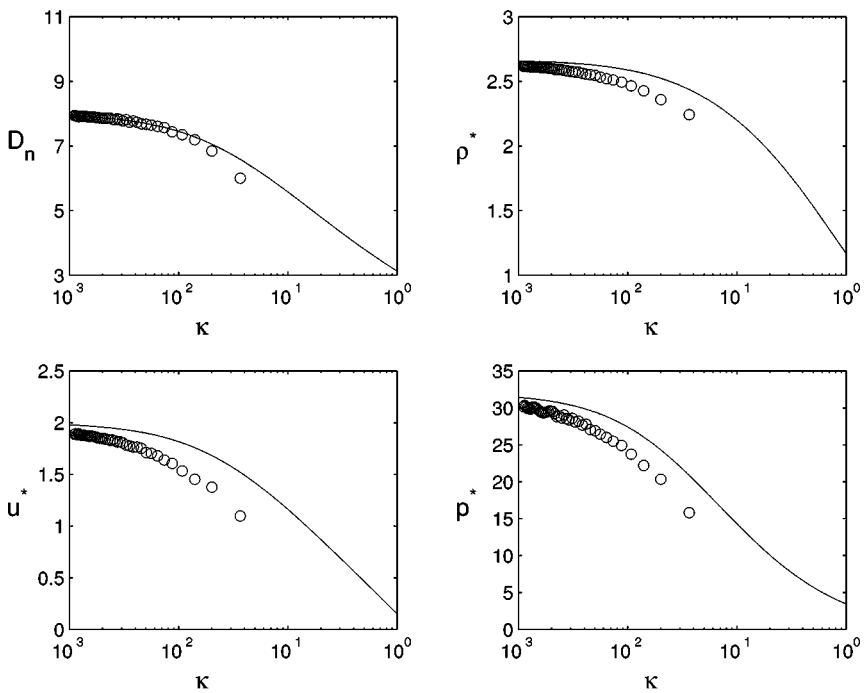

FIG. 31. Plot of D_n and the sonic ($*$) states as a function of κ for DSD (solid) and model MPB-3b (circles) with $\Delta x = 0.5$ mm.

6. CONCLUSIONS

We have presented a comprehensive review of the traditional, pressure-based program burn algorithm and have compared solutions to those of a direct numerical simulation. It was shown that if curvature is present, the TPB alogrithm overpredicts the shock speed. A slight modification to the burn times, based on detonation shock dynamic theory, can correct the shock speed difficulty. Various models are presented and compared to DNS; overall, the results of Model II (constant upstream value for the internal energy, fixing the program burn reaction zone length) give results which surprisingly capture the DNS structure, even with a grid resolution of about five times larger than that of the DNS. We are currently investigating these models in two-dimensional geometries and extension to real product equations of state.

ACKNOWLEDGMENTS

The work of D. S. Stewart was supported by the Department of Energy, DOE-LANL under the present contract I2933-0019 and previous Contracts with LANL. T. L. Jacson was supported by a previous LANL contract and the DOE contract that supports the UIUC ASCI center, Center for Simulation of Advanced Rockets. J. B. Bdzil is supported at Los Alamos by the Department of Energy.

REFERENCES

1. W. C. Davis, Introduction to explosive, in *Explosive Effects and Applications*, edited by J. A. Zukas and W. P. Walter, (Springer Verlag, Bérlin/New York, 1998), Ch. 1.
2. W. Fickett and W. C. Davis, *Detonation: Theory and Experiment* (Dover, New York, 2000).
3. D. S. Stewart and J. B. Bdzil, The shock dynamics of stable multi-dimensional detonation, *Combust. Flame.* **72**, 311 (1988).
4. J. B. Bdzil and D. S. Stewart, Modeling of two-dimensional detonation with detonation shock dynamics, *Phys. Fluids, A* **1**, 1261 (1988).
5. D. S. Stewart, The dynamics of multi-dimensional detonation in gaseous and condensed phases explosives: Topical review, in *Proceedings of the 27th (International) Conference on Combustion* (The Combustion Institute, 1998), pp. 2189–2205.
6. T. D. Aslam, J. B. Bdzil, and D. S. Stewart, Level set methods applied to modeling detonation shock dynamics, *J. Comput. Phys.* **126** (1996).
7. T. D. Aslam and D. S. Stewart, Detonation shock dynamics and comparisons with direct numerical simulation, *Combust. Theory Model*. **3**, 77 (1999).
8. T. D. Aslam, J. B. Bdzil, and L. Hill, Extensions to DSD-theory: Analysis of PBX9502 rate stick data, in *Proceedings of the Eleventh (International) Symposium on Combustion* (2000), pp. 21–29. Also appears as Los Alamos National Laboratory Technical Release LA-UR-98-3884 (1998).
9. J. B. Bdzil, T. D. Aslam, and D. S. Stewart, *Resolved 3D Detonation Reaction Zones: Memory and Time Requirements for DNS*. Los Alamos Report LA-UR-97-792 (Los Alamos National Laboratory, Los Alamos, NM, 1997).
10. G. S. Jiang and C. Shu, Efficient implementation of weighted ENO schemes, *J. Comput. Phys*. **126**, 202 (1996).
11. C. Shu and S. Osher, Efficient implementation of essentially non-oscillatory shock-capturing schemes, *J. Comput. Phys*. **77**, 439 (1988).
12. G. B. Whitham, *Linear and Nonlinear Waves* (Wiley-Interscience, New York, 1974), p. 277.
13. M. L. Wilkins, Calculation of elastic-plastic flow, in *Methods in Computational Physics, Advances in Research and Applications*, Fundamental Methods in Hydro-dynamics, edited by B. Alder, S. Fernbach, and M. Rotenberg, (Academic Press, San Diego, 1964), Vol. 3, pp. 211–262.
14. S. Xu, T. D. Aslam, and D. S. Stewart, High resolution numerical simulation of ideal and non-ideal compressible reacting flows with embedded boundaries, *Combust. Theory Model*. **1**, 113 (1997).